

Supplementary Information:

Carbon Capture: Theoretical Guidelines for Activated Carbon-based CO₂ Adsorption Material Evaluation

Drew M. Glenna^{#a}, Asmita Jana^{#b, c}, Qiang Xu^b, Yixiao Wang^{d, e}, Yuqing Meng^d, Yingchao Yang^{f, g}, Manish Neupane^{f, g}, Lucun Wang^d, Haiyan Zhao^{*a, h}, Jin Qian^{*b}, and Seth W. Snyder^{*d}

^a Department of Nuclear Engineering & Industrial Management, University of Idaho, Idaho Falls, ID 83402, USA

^b Chemical Sciences Division, Lawrence Berkeley National Laboratory, Berkeley, CA 94720, USA

^c Advanced Light Source, Lawrence Berkeley National Laboratory, Berkeley, CA 94720, USA

^d Energy & Environmental Science and Technology, Idaho National Laboratory, Idaho Falls, ID 83415, USA

^e Current Address: School of Physical Science and Technology, ShanghaiTech University, Shanghai, 201210, China

^f Department of Mechanical Engineering, University of Maine, Orono, ME 04469, USA

^g Current Address: Mechanical & Aerospace Engineering, College of Engineering, University of Missouri, Columbia, MO 65201, USA

^h Department of Chemical and Biological Engineering, University of Idaho, Idaho Falls, ID 83402, USA

E-mail: haiyanz@uidaho.edu, jqian2@lbl.gov, seth.snyder@inl.gov

Table of Contents

Computational Methods.....	5
Geometry Set Up	5
DFT Calculation Method	5
Charge Analysis Method	5
Physisorption-Chemisorption Boundary on Graphene Materials.....	6
Summary of the state-of-the-art DFT calculation results on graphene derivatives	6
Figure S1. Current state-of-the-art DFT calculations of CO ₂ E _{ads} on PG, DG, FG, MG, and Stone-Wales defect (SWG) graphene	7

CO ₂ E _{ads} on Mg-MOF-74.....	7
Figure S2. CO ₂ E _{ads} on Mg-MOF-74	8
CO ₂ Adsorption on Doped Graphene (DG).....	8
Table S1. CO ₂ E _{ads} on PG and DG with shortest atomic distances.....	8
Figure S3. Ionically relaxed CO ₂ configuration on PGT (a, b) and PGH (c, d) sites	9
Figure S4. Ionically relaxed CO ₂ configuration on NGT1 (a, b), NGT2 (c, d), NGT3 (e, f), NGTP (g, h), and NGH (i, j) sites.....	10
Figure S5. Ionically relaxed CO ₂ configuration on FeGT (a, b), FeGTP (c, d), and FeGH (e, f) sites.....	10
Figure S6. Ionically relaxed CO ₂ configuration on CoGT (a, b) and CoGH (c, d) sites	11
Figure S7. Ionically relaxed CO ₂ configuration on NiGT1 (a, b), NiGT2 (c, d), NiGH1 (e, f), and NiGH2 (g, h) sites	11
Figure S8. Ionically relaxed CO ₂ configuration on CuGT1 (a, b), CuGT2 (c, d), CuGH1 (e, f), CuGH2 (g, h), and CuGH3 (i, j) sites	12
CO ₂ Adsorption on Functionalized Graphene (FG)	12
Table S2. FMs E _{ads} on PG with shortest atomic distances.....	14
Table S3. CO ₂ E _{ads} on FG with shortest atomic distances between FM and CO ₂ (elements are in parentheses if a bond is formed), CO ₂ and PG (y (vacuum) direction), and FM and PG.....	15
Figure S9. Ionically relaxed CO on PG	16
Figure S10. Ionically relaxed OH on PG	16
Figure S11. Ionically relaxed COOH on PG.....	16
Figure S12. Ionically relaxed NH ₂ configuration on PG in NH ₂ T (a, b), NH ₂ H (c, d), and NH ₂ B (e, f) sites.....	17
Figure S13. Ionically relaxed NH ₂ CH ₃ configuration on PG in NH ₂ CH ₃ T1 (a, b), NH ₂ CH ₃ T2 (c, d), NH ₂ CH ₃ T3 (e, f), NH ₂ CH ₃ T4 (g, h), NH ₂ CH ₃ H1 (i, j), NH ₂ CH ₃ H2 (k, l), NH ₂ CH ₃ H3 (m, n), NH ₂ CH ₃ B1 (o, p), and NH ₂ CH ₃ B2 (q, r) sites.....	17
Figure S14. Ionically relaxed NHCH ₃ configuration on PG in NHCH ₃ T1 (a, b) and NHCH ₃ T2 (c, d) sites	18
Figure S15. Ionically relaxed NH ₂ CH ₂ configuration on PG in NH ₂ CH ₂ T (a, b) site.....	18
Figure S16. Ionically relaxed C ₅ H ₅ N configuration on PG in C ₅ H ₅ NT (a, b), C ₅ H ₅ NH (c, d), and C ₅ H ₅ NB (e, f) sites	18
Figure S17. Ionically relaxed C ₆ H ₅ NH ₂ configuration on PG in C ₆ H ₅ NH ₂ H1 (a, b), C ₆ H ₅ NH ₂ H2 (c, d), and C ₆ H ₅ NH ₂ B (e, f) sites.....	19
Figure S18. Ionically relaxed CH ₅ N ₃ configuration on PG in CH ₅ N ₃ TT (a, b), CH ₅ N ₃ TH (c, d), CH ₅ N ₃ HT (e, f), and CH ₅ N ₃ HB (g, h) sites	19

Figure S19. Ionically relaxed C ₃ N ₂ H ₄ configuration on PG in C ₃ N ₂ H ₄ T1 (a, b), C ₃ N ₂ H ₄ T2 (c, d), C ₃ N ₂ H ₄ TT1 (e, f), C ₃ N ₂ H ₄ TT2 (g, h), C ₃ N ₂ H ₄ TT3 (i, j), and C ₃ N ₂ H ₄ H (k, l) sites	20
Figure S20. Ionically relaxed CO ₂ configuration on COG	20
Figure S21. Ionically relaxed CO ₂ configuration on OHGT (a, b) and OHGi (c, d) sites	20
Figure S22. Ionically relaxed CO ₂ configuration on COOHG1 (a, b (xy plane)) and COOHG2 (c, d) sites	21
Figure S23. Ionically relaxed CO ₂ configuration on NH ₂ GT1 (a, b), NH ₂ GT2 (c, d), NH ₂ Gi1 (e, f), and NH ₂ Gi2 (g, h) sites	21
Figure S24. Ionically relaxed CO ₂ configuration on NH ₂ CH ₃ GT (a, b), NH ₂ CH ₃ Gi1 (c, d), NH ₂ CH ₃ Gi2 (e, f), and NH ₂ CH ₃ Gi3 (g, h) sites	22
Figure S25. Ionically relaxed CO ₂ configuration on C ₅ H ₅ NGT (a, b), C ₅ H ₅ NGi1 (c, d), and C ₅ H ₅ NGi2 (e, f) sites.....	22
Figure S26. Ionically relaxed CO ₂ configuration on C ₆ H ₅ NH ₂ GT1 (a, b), C ₆ H ₅ NH ₂ GT2 (c, d), C ₆ H ₅ NH ₂ Gi1 (e, f), C ₆ H ₅ NH ₂ Gi2 (g, h), and C ₆ H ₅ NH ₂ Gi3 (i, j) sites	23
Figure S27. Ionically relaxed CO ₂ configuration on CH ₅ N ₃ GT (a, b), CH ₅ N ₃ Gi1 (c, d), CH ₅ N ₃ Gi2 (e, f), and CH ₅ N ₃ Gi3 (g, h) sites	24
Figure S28. Ionically relaxed CO ₂ configuration on C ₃ N ₂ H ₄ GT (a, b), C ₃ N ₂ H ₄ Gi1 (c, d), and C ₃ N ₂ H ₄ Gi2 (e, f) sites	24
CO ₂ Adsorption on Monovacancy Defect Graphene (MG)	24
Table S4. FMs E _{ads} on MG with shortest atomic distances	25
Table S5. CO ₂ E _{ads} on FG on MG with shortest atomic distances between FM and CO ₂ (elements are in parentheses if a bond is formed), CO ₂ and PG (y (vacuum) direction), and FM and PG	25
Figure S29. Ionically relaxed NH ₂ CH ₃ configuration on MG in NH ₂ CH ₃ MG1 (a, b) and NH ₂ CH ₃ MG2 (c, d) sites.....	26
Figure S30. Ionically relaxed C ₅ H ₅ N configuration on MG in C ₅ H ₅ NMGT1 (a, b), C ₅ H ₅ NMGT2 (c, d), C ₅ H ₅ NMGH (e, f), C ₅ H ₅ NMGB1 (g, h), C ₅ H ₅ NMGB2 (i, j), and C ₅ H ₅ NMGB3 (k, l) sites	26
Figure S31. Ionically relaxed CO ₂ configuration on MG1 (a, b), MG2 (c, d), MG3 (e, f), and MG4 (g, h) sites	27
Figure S32. Ionically relaxed CO ₂ configuration on MG1NH ₂ CH ₃ (a, b) and MG2NH ₂ CH ₃ (c, d) sites	27
Figure S33. Ionically relaxed CO ₂ configuration on MGC ₅ H ₅ NT1 (a, b), MGC ₅ H ₅ NT2* (c, d), MGC ₅ H ₅ Ni1 (e, f), MGC ₅ H ₅ Ni2 (g, h), and MGC ₅ H ₅ Ni3 (i, j) sites	28
Selectivity with E _{ads}	28
Table S6. N ₂ , O ₂ , and H ₂ O E _{ads} on FG with shortest atomic distances between FM and gas (elements are in parentheses if a bond is formed), gas and PG (y (vacuum) direction), and FM and PG.....	28

Figure S34. Ionically relaxed H ₂ O configuration on PG in H ₂ OGT (a, b), H ₂ OGH (c, d), and H ₂ OGB (e, f) sites	30
Figure S35. Ionically relaxed H ₂ O configuration on GNH ₂ CH ₃ in H ₂ OGNH ₂ CH ₃ T (a, b), H ₂ OGNH ₂ CH ₃ i1 (c, d), and H ₂ OGNH ₂ CH ₃ i2 (e, f) sites	30
Figure S36. Ionically relaxed H ₂ O configuration on GC ₅ H ₅ N in H ₂ OGC ₅ H ₅ NT1 (a, b), H ₂ OGC ₅ H ₅ NT1 (c, d), H ₂ OGC ₅ H ₅ Ni1 (e, f), and H ₂ OGC ₅ H ₅ Ni2 (g, h) sites	31
Figure S37. Ionically relaxed O ₂ configuration on PG in O ₂ GT (a, b), O ₂ GH (c, d), and O ₂ GB (e, f) sites	31
Figure S38. Ionically relaxed O ₂ configuration on GNH ₂ CH ₃ in O ₂ GNH ₂ CH ₃ T (a, b), O ₂ GNH ₂ CH ₃ i1 (c, d), and O ₂ GNH ₂ CH ₃ i2 (e, f) sites	32
Figure S39. Ionically relaxed O ₂ configuration on GC ₅ H ₅ N in O ₂ GC ₅ H ₅ NT1 (a, b), O ₂ GC ₅ H ₅ NT2* (c, d), O ₂ GC ₅ H ₅ Ni1* (e, f), and O ₂ GC ₅ H ₅ Ni2 (g, h) sites.....	33
Figure S40. Ionically relaxed N ₂ configuration on PG in N ₂ GT1 (a, b), N ₂ GT2 (c, d), N ₂ GH1 (e, f), N ₂ GH2 (g, h), and N ₂ GB (i, j) sites	33
Figure S41. Ionically relaxed N ₂ configuration on GNH ₂ CH ₃ in N ₂ GNH ₂ CH ₃ T (a, b), N ₂ GNH ₂ CH ₃ i1 (c, d), and N ₂ GNH ₂ CH ₃ i2 (e, f) sites	33
Figure S42. Ionically relaxed N ₂ configuration on GC ₅ H ₅ N in N ₂ GC ₅ H ₅ NT1 (a, b), N ₂ GC ₅ H ₅ NT1 (c, d), N ₂ GC ₅ H ₅ Ni1* (e, f), and N ₂ GC ₅ H ₅ Ni2 (g, h) sites.....	34
Coadsorption with E _{ads}	34
Table S7. CO ₂ E _{ads} on H ₂ O adsorbed FG with shortest atomic distances between FM and gas (elements are in parentheses if a bond is formed), gas and PG (y (vacuum) direction), and FM and PG.....	35
Figure S43. Ionically relaxed CO ₂ configuration on H ₂ OGNH ₂ CH ₃ in CO ₂ :H ₂ OGNH ₂ CH ₃ i (a, b) site	35
Figure S44. Ionically relaxed CO ₂ configuration on H ₂ OGC ₅ H ₅ N in CO ₂ :H ₂ OGC ₅ H ₅ NT (a, b), CO ₂ :H ₂ OGC ₅ H ₅ Ni1 (c, d), CO ₂ :H ₂ OGC ₅ H ₅ Ni2 (e, f), CO ₂ :H ₂ OGC ₅ H ₅ Ni3 (g, h), and CO ₂ :H ₂ OGC ₅ H ₅ Ni4 (i, j) sites	36
Figure S45. Ionically relaxed H ₂ CO ₃ configuration on GC ₅ H ₅ N in H ₂ CO ₃ GC ₅ H ₅ Ni (a, b) site	36
Coverage Effects on CO ₂ E _{ads}	36
Table S8. CO ₂ E _{ads} (eV) on PG, NH ₂ CH ₃ -FG, and C ₅ H ₅ N-FG with respect to coverage	37
Figure S46. Single point configuration of CO ₂ on PG in 36 (a), 252 (b), 780 (c), and 1152 (d) C atom sheets using ARES	38
Figure S47. Single point configuration of CO ₂ on GNH ₂ CH ₃ in 36 (a), 60 (b), and 96 (c) C atom sheets using QE	38
Figure S48. Single point configuration of CO ₂ on GC ₅ H ₅ N in 36 (a), 60 (b), and 96 (c) C atom sheets using QE	39

Van der Waals and Electrostatic Contributions in CO ₂ E _{ads}	39
Table S9. Interaction energies (eV) of CO ₂ with FMs and PG.....	39
Bader Charge Analysis	40
Table S10. Bader Charge Difference (BCD (e)) for NH ₂ -T FG	40
Table S11. BCD (e) for C ₆ H ₅ NH ₂ -I FG	41
Table S12. BCD (e) for C ₅ H ₅ N-I FG	42
Table S13. BCD (e) for NH ₂ CH ₃ -I FG	44
Table S14. BCD (e) for CH ₅ N ₃ -I FG	45
Table S15. BCD (e) for NH ₂ -I FG	46

Computational Methods

Geometry Set Up

A single layer of pristine graphene (PG) is modeled using the Atomic Simulation Environment¹ (ASE) as a $3 \times 3 \times 1$ supercell with 36 C atoms. The PG layer is modeled as a sheet with x and z being the periodic directions. To avoid interactions between PG sheets a vacuum gap of 15 Å is employed in the y axis. The lattice parameter is set to 2.452 Å determined by an ionic and volume relaxation calculation. For consistency, CO₂, N₂, O₂, H₂O, and all the functional molecules (FMs) are modeled in the same cell dimensions ($7.36 \times 12.90 \times 15.00 \text{ \AA}^3$) as the 36 C atom sheet. Six different sizes (36, 60, 96, 252, 780, and 1152) of C atom sheets were generated with ASE's set PG structure (1.42 Å C-C distance) to study coverage effects. Each of the 252, 780, and 1152 C atom sheets contain a 5 Å vacuum gap in the x axis, with the dangling edge C atoms saturated with H atoms, to minimize computational cost. The atomic positions of the ionically relaxed methylamine and pyridine FMs (along with CO₂) on PG were used in the 36, 60 and 96 C atom sheet coverage calculations.

DFT Calculation Method

Spin Polarized DFT calculations are performed in Quantum Espresso²⁻⁴ (QE) with van der Waals forces (Grimmes D2)^{5,6} to account for long range London dispersion interactions between the adsorbent and adsorbates. Plane-wave basis sets for the valence electron eigenfunctions are used with the projector-augmented⁷ method along with the generalized gradient approximation exchange functional by Perdew-Burke-Enzerhof.⁸ Gaussian smearing is employed with a smearing width of 0.001 Ry. A Monkhorst-Pack k-point grid of $2 \times 1 \times 1$ with a kinetic energy cutoff of 100 Ry was used for the ionic and volume relaxation calculations with pristine and doped graphene. In these calculations, the x and z directions of the graphene sheet are relaxed to a pressure of 0 bar with a convergence threshold of 0.5 bar. The total energy and force convergence threshold for ionic minimization is 2.72×10^{-3} eV and 2.72×10^{-2} eV, respectively. The total energy convergence threshold for self-consistency is 2.72×10^{-5} eV. A k-point grid of $4 \times 2 \times 2$ and a kinetic energy cutoff of 85 Ry achieved <1 meV/atom convergence for all structures and molecules. The latter grid and cutoff are implemented in all the ionic relaxation and self-consistent field calculations for

the adsorption energy (E_{ads}) calculations in this work. For coverage effects, single point calculations with a gamma point and an 85 Ry cutoff was used.

Charge Analysis Method

Three methods are used to further indicate and describe electron interactions and the type of bonding. First, the interaction distances between CO₂ and the graphene derivative is analyzed to determine if the dominant forces are either van der Waals, Coulombic, or chemical bonding. Second, Bader charge^{9–12} is used to determine the depletion and augmentation of charge on the atoms. Third, the charge density difference of CO₂ and the graphene derivative is plotted using VESTA¹³ to provide further insight into the depletion and augmentation of charge by visualizing their charge density before and after CO₂ is introduced.

Physisorption-Chemisorption Boundary on Graphene Materials

From a physical chemistry perspective, physisorption typically corresponds to non-bonding interactions like van der Waals whereas chemisorption often involves a significant charge transfer accompanied with formation of chemical bonds. More practically, the boundary between physisorption and chemisorption is commonly accepted to be in the range of -0.41 to -0.51 eV,¹⁴ and we found it to be apt for our system. For instance, the CO₂ adsorption energy of methylamine functionalized graphene is right below the physisorption-chemisorption boundary (-0.367 eV), and we found that there was no N-C bond formed with a distance of 2.893 Å (see Table S3). In addition, CO₂ exhibited no Bader charge transfer with methylamine (see Table S13). On the other hand, imidazole functionalized graphene adsorbed CO₂ with an energy just above the physisorption-chemisorption boundary (-0.574 eV) and formed a N-C bond with a distance of 1.611 Å (see Table S3). Furthermore, CO₂ and imidazole showed Bader charge transfer with N (of C₃N₂H₄), C (of CO₂), O1 (of CO₂), and O2 (of CO₂) gaining -0.45, 0.21, 0.11, and 0.07 e, respectively. A similar CO₂ adsorption energy range (-0.41 to -0.78 eV) is commonly accepted for direct air capture applications.^{15,16}

Summary of the state-of-the-art DFT calculation results on graphene derivatives

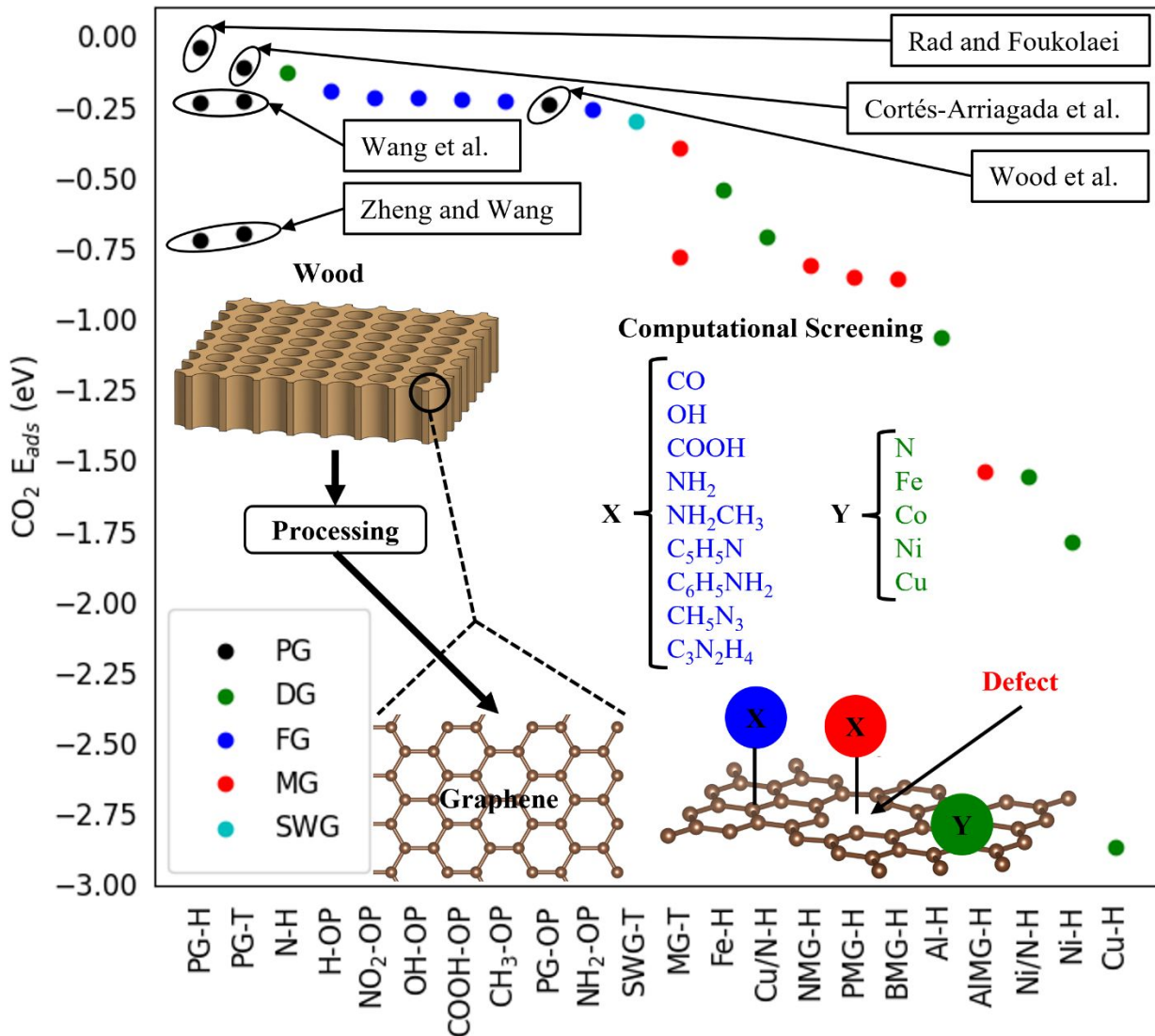


Figure S1. Current state-of-the-art DFT calculations of $\text{CO}_2 E_{\text{ads}}$ on PG, DG, FG, MG, and Stone-Wales defect (SWG) graphene¹⁷⁻²¹ with the process schematic of wood to graphene on the nanoscale including our evaluation of DG, FG, and MG.

$\text{CO}_2 E_{\text{ads}}$ on Mg-MOF-74

To base off of the ideal $\text{CO}_2 E_{\text{ads}}$ that is neither too large nor too small, we turned to calculation of the CO_2 adsorption on the current state-of-the-art solid sober solution: Mg-MOF-74.²²⁻²⁷ MOF-74 or $M_2(\text{dobdc})$ ($H_4\text{dobdc} = 2,5\text{-dihydroxyterephthalic acid}$; $M = \text{Mg, Co, Ni, Zn, Mn, Fe}$) is a benchmark framework with outstanding adsorption properties for a range of applications, including carbon capture. The structure of MOF-74 is generally described as hexagonal honeycomb channels with accessible open metal sites. CO_2 is absorbed through the interaction of O and the Mg site. The $\text{CO}_2 E_{\text{ads}}$ at the same PBE-D2 level of calculation is -0.41 eV, in good agreement with the results from Vlaisavljevich et.al and Lee et.al.^{28,29}

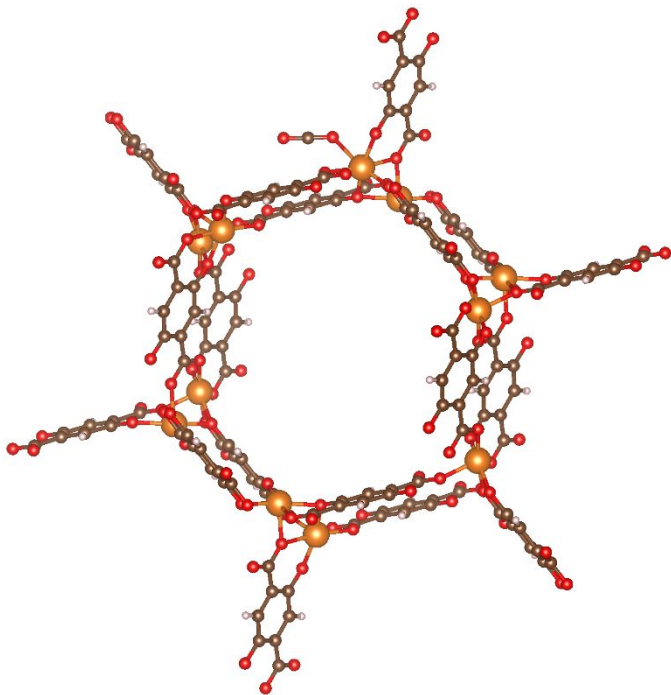


Figure S2. $\text{CO}_2 E_{\text{ads}}$ on Mg-MOF-74.

CO_2 Adsorption on Doped Graphene (DG)

We considered substitutionally doping N, Fe, Co, Ni, and Cu in graphene as potential materials to reach our target $\text{CO}_2 E_{\text{ads}}$. An ionic relaxation of CO_2 in the top (Tx) and hollow (Hx) sites for each dopant is conducted to determine the most stable adsorption site (see Table S1 and Figures S3-S8). As a baseline, CO_2 adsorbed on PG is the most stable in the T site (-0.250 eV with a 3.202 Å CO_2 -PG distance), which is in excellent agreement with other computational and experimental works^{17-18, 30}. As PG is less stable than our target we moved to N-DG where CO_2 was placed in three different T sites (initially 1.3-2 Å N-C distance) to see if a N-C bond would form. However, there are weak interactions between N-C (of CO_2) and a chemical bond does not form. Overall, CO_2 is less stable on N-DG (-0.199 eV in hollow site) than PG and results in a shortest atomic distance of 3.108 Å (in agreement with Wang et al.)¹⁷. Both PG and N-DG physisorb CO_2 (primarily vdW interactions), while the transition metal dopants chemisorb CO_2 . CO_2 is most stable in the H site for each of the transition metal dopants (Fe, Co, Ni, and Cu). In order of least to most energetically stable CO_2 interaction: Cu, Ni, Co, and Fe-DG result in a CO_2 -dopant distance of 2.457, 2.423, 2.276, and 2.097 Å, respectively. However, the transition metal dopants interact much more strongly with CO_2 than our target $\text{CO}_2 E_{\text{ads}}$ (see Table S1).

Table S1. $\text{CO}_2 E_{\text{ads}}$ on PG and DG with shortest atomic distances (y (vacuum) direction for PG and elements are in parentheses if a bond is formed). Gray indicates the most stable CO_2 site.

Dopant/G/Site	E_{ads} (eV)	vdW E_{ads} (eV)	CO_2 -Dopant (Å)
PGT	-0.250	-0.175	3.202

PGH	-0.239	-0.158	3.282
NGT1	-0.188	-0.177	3.186
NGT2	-0.188	-0.176	3.188
NGT3	-0.190	-0.177	3.179
NGTP	-0.157	-0.095	3.013
NGH	-0.199	-0.178	3.108
FeGT	-2.531	-0.206	2.017 (C)
FeGTP	-2.570	-0.131	2.046 (O)
FeGH	-2.614	-0.192	2.097 (O)
CoGT	-2.348	-0.196	4.062
CoGH	-2.459	-0.236	2.276 (O)
NiGT1	-2.132	-0.211	4.010
NiGT2	-2.046	-0.132	3.164
NiGH1	-2.103	-0.186	4.131
NiGH2	-2.198	-0.244	2.423 (O)
CuGT1	-1.384	-0.227	4.042
CuGT2	-1.334	-0.130	2.488 (O)
CuGH1	-1.364	-0.183	4.503
CuGH2	-1.431	-0.223	2.380 (O)
CuGH3	-1.433	-0.242	2.457 (O)

For the following figures, the odd columns are the xz plane view and the even columns are the yz plane view (unless specified otherwise). The most stable adsorption geometry is indicated by the red box.

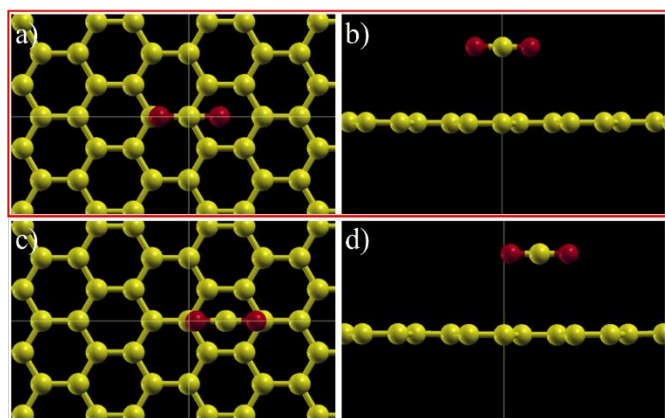


Figure S3. Ionically relaxed CO₂ configuration on PGT (a, b) and PGH (c, d) sites.

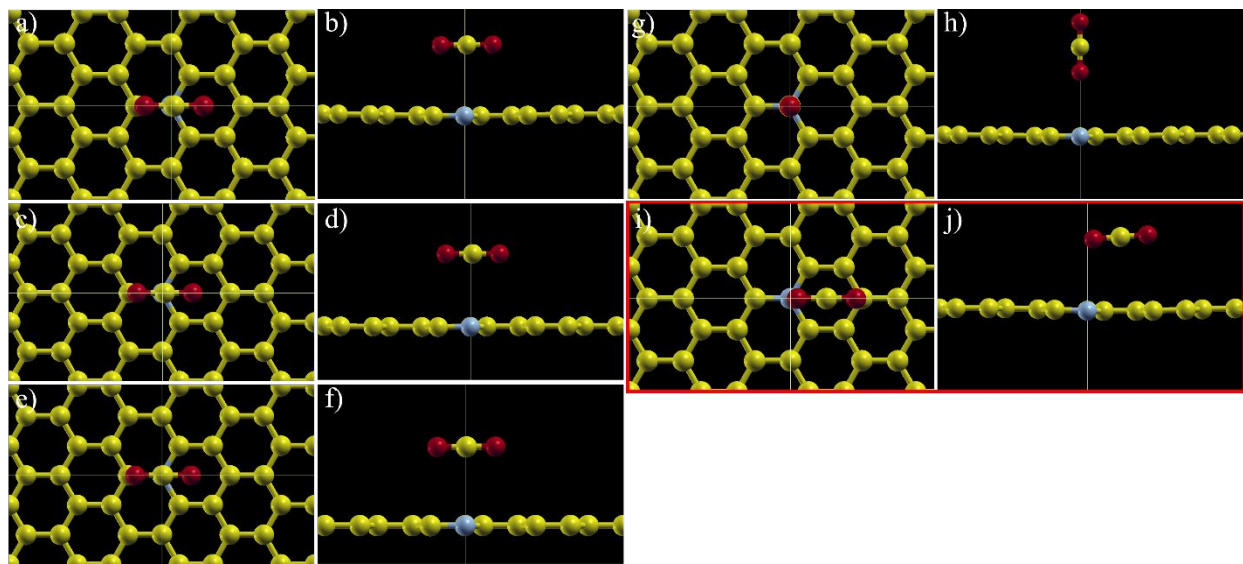


Figure S4. Ionically relaxed CO_2 configuration on NGT1 (a, b), NGT2 (c, d), NGT3 (e, f), NGTP (g, h), and NGH (i, j) sites.

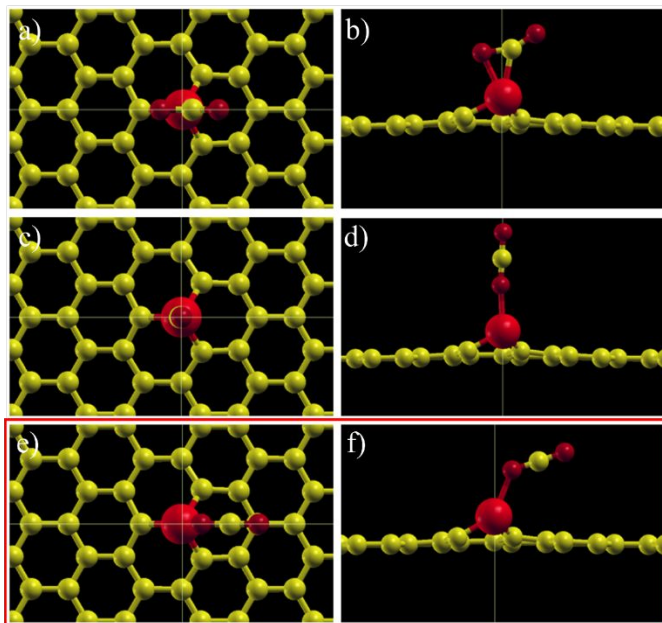


Figure S5. Ionically relaxed CO_2 configuration on FeGT (a, b), FeGTP (c, d), and FeGH (e, f) sites.

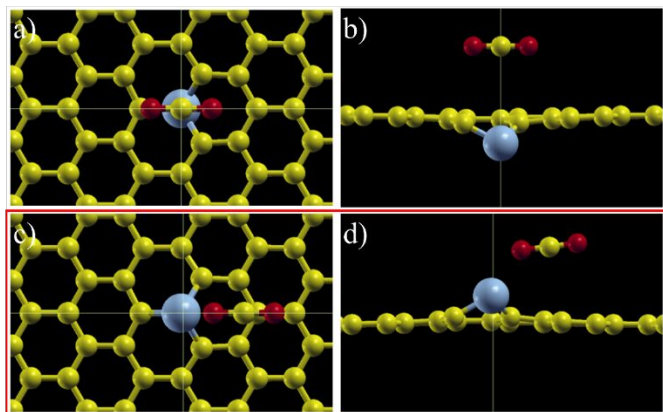


Figure S6. Ionically relaxed CO_2 configuration on CoGT (a, b) and CoGH (c, d) sites.

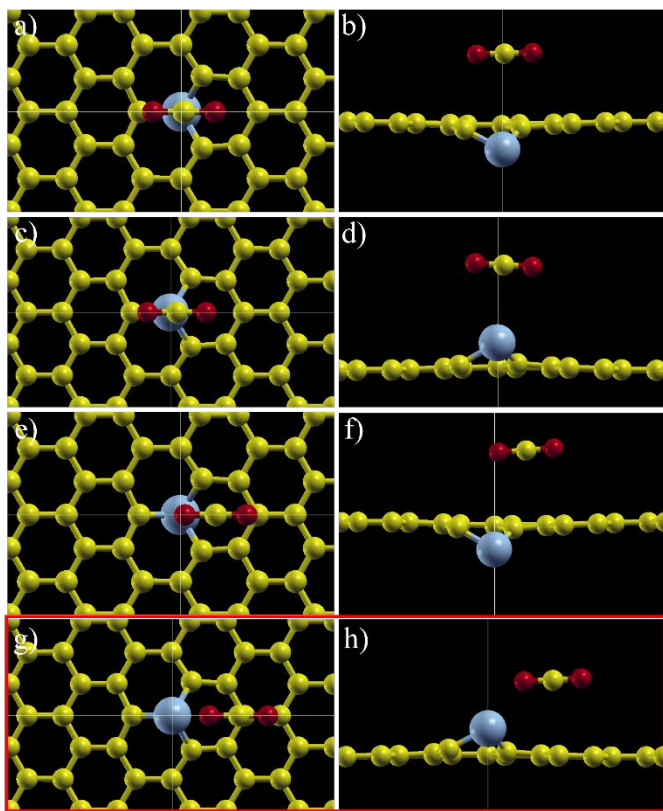


Figure S7. Ionically relaxed CO_2 configuration on NiGT1 (a, b), NiGT2 (c, d), NiGH1 (e, f), and NiGH2 (g, h) sites.

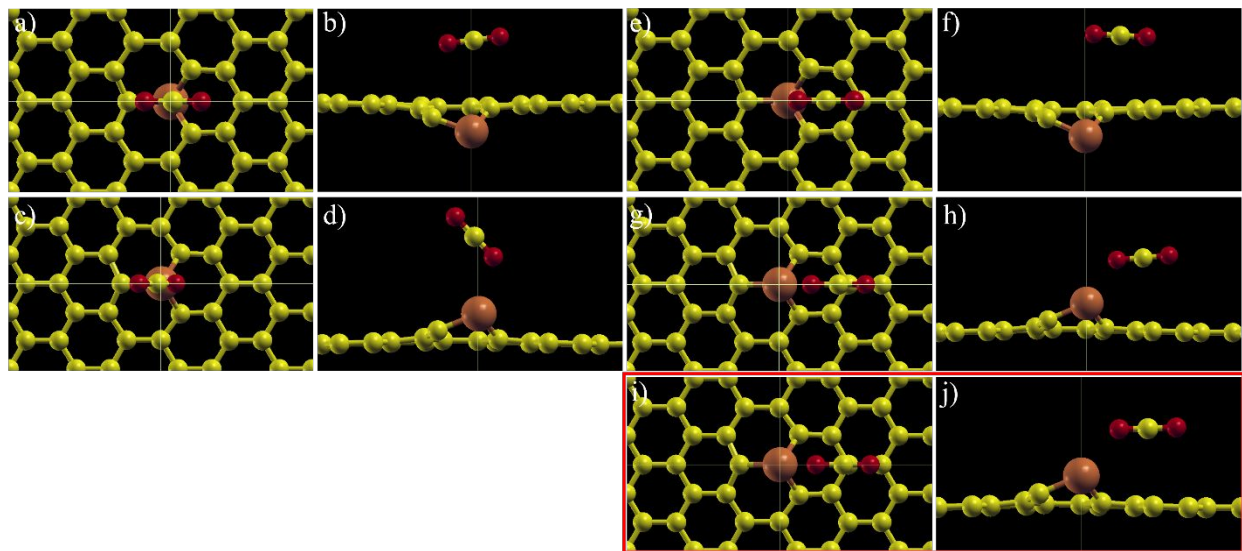


Figure S8. Ionically relaxed CO_2 configuration on CuGT1 (a, b), CuGT2 (c, d), CuGH1 (e, f), CuGH2 (g, h), and CuGH3 (i, j) sites.

CO_2 Adsorption on Functionalized Graphene (FG)

CO , OH , COOH , NH_2 , NH_2CH_3 , $\text{C}_5\text{H}_5\text{N}$, $\text{C}_6\text{H}_5\text{NH}_2$, CH_5N_3 , and $\text{C}_3\text{N}_2\text{H}_4$ FMs were adsorbed on PG in the basal plane and screened as potential materials to reach our target $\text{CO}_2 E_{\text{ads}}$ (see Table S2 and Figures S9-S19 for FMs E_{ads} and geometry; see Table S3 and Figures S20-S28 for $\text{CO}_2 E_{\text{ads}}$ on FG and geometry). To the best of our knowledge, predicting CO , NH_2CH_3 , $\text{C}_5\text{H}_5\text{N}$, $\text{C}_6\text{H}_5\text{NH}_2$, CH_5N_3 , and $\text{C}_3\text{N}_2\text{H}_4$ adsorbing on PG and interacting with CO_2 on PG is a first of a kind. The logic of the selection has been discussed in the following three paragraphs. An ionic relaxation of each FM (and PG) in the T, H, and/or bridge (Bx) sites on PG was conducted to determine the most stable site. The H and B sites were not considered if a chemical bond was formed between the FM and PG (T site). Further, CO_2 was ionically relaxed (along with the FM and PG) on top of (Tx) and inserted (ix) next to the FM on PG to determine the most stable site.

First, we started with O-containing FMs adsorption with CO_2 on PG. CO is most stable physisorbing on PG in the T site with an E_{ads} of -0.201 eV and a 3.245 Å FM-PG distance. Then we add CO_2 into the cell, which adsorbs above CO by weak physisorption (-0.058 eV and 3.260 Å CO_2 -FM distance). Next, we look at COOH FM which forms a C-C bond (1.609 Å) with PG in the T site (-0.402 eV). CO_2 is most stable physisorbing on top of COOH with an E_{ads} of -0.220 eV and a 1.911 Å O-H distance (excellent agreement with literature)¹⁸. We continue our search toward our target by moving to the OH FM, which forms a C-O bond (1.507 Å) with PG in the T site (-0.960 eV). CO_2 physisorbs to the OH FG in the T site with an E_{ads} of -0.152 eV and a CO_2 -FM distance of 2.447 Å (in agreement with literature)¹⁸. However, inserting CO_2 next to OH results in the C-O bond breaking between OH and PG and forming bicarbonate with CO_2 (-0.643 eV and 1.375 Å CO_2 -FM distance). In all, CO , COOH , and OH FG drive $\text{CO}_2 E_{\text{ads}}$ farther away from our target and are not further pursued in this study.

Second, we moved to N-containing FMs in hopes of reaching our target $\text{CO}_2 E_{\text{ads}}$. We started with NH_2 , which is most stable in the T site (-0.321 eV) on PG with the formation of a N-C bond (1.473 Å). CO_2 is then introduced into the cell and adsorbs above NH_2 with weak physisorption (-0.096 eV and 2.634 Å CO_2 -FM distance), which is lower than predicted on edge FG (-0.260 eV)¹⁸. This is expected as CO_2 has minimal interaction with PG as it is directly above NH_2 and 5 Å above PG. However, inserting CO_2 next to NH_2 breaks the N-C bond between NH_2 and PG and forms a N-C bond (1.390 Å) with CO_2 (-0.979 eV). Since the T1 and i1 CO_2 adsorption sites on NH_2 FG are much less and more stable than our target, respectively, we transitioned to NH_2CH_3 to decrease the electronegativity (EN) difference between CO_2 and the FM. NH_2CH_3 is most stable in the T1 site with an E_{ads} of -0.265 eV and a 2.698 Å FM-PG distance. CO_2 adsorbs above NH_2CH_3 with weak physisorption (-0.078 eV and 2.776 Å CO_2 -FM distance). However, the most stable CO_2 site is the i2 site, which is near our target $\text{CO}_2 E_{\text{ads}}$ (-0.367 eV and 2.893 Å CO_2 -FM distance) due to dipole-dipole interactions.

We continued our search for additional FMs to reach our target $\text{CO}_2 E_{\text{ads}}$ and shifted to aromatic molecules. We started with $\text{C}_5\text{H}_5\text{N}$ which is most stable in the H site due to π - π interactions (with PG) with an E_{ads} of -0.543 eV (mostly vdW interactions -0.516 eV) and a 3.228 Å FM-PG distance. Note, $\text{C}_5\text{H}_5\text{N}$ is more stable on PG than our target $\text{CO}_2 E_{\text{ads}}$ indicating thermal stability. Then we introduce CO_2 into the cell where CO_2 adsorbs above $\text{C}_5\text{H}_5\text{N}$ by weak physisorption (-0.129 eV and 3.192 Å CO_2 -FM distance), which is in excellent agreement with literature³¹ on CO_2 interacting above $\text{C}_5\text{H}_5\text{N}$ without PG as the vdW interactions between CO_2 and PG are minimal at 6.391 Å. For inserting CO_2 , the i1 site is the most stable and is near our target $\text{CO}_2 E_{\text{ads}}$ (-0.347 eV and 2.758 Å CO_2 -FM distance) due to dipole-dipole interactions. Next, we moved to $\text{C}_6\text{H}_5\text{NH}_2$, which is most stable on PG in the H site (π - π interactions) and is more thermally stable than $\text{C}_5\text{H}_5\text{N}$ on PG (-0.633 eV and 2.937 Å FM-PG distance). CO_2 physisorbs above $\text{C}_6\text{H}_5\text{NH}_2$ with an E_{ads} of -0.170 eV and a 2.888 Å CO_2 -FM distance. Interestingly, the inserted sites cease to improve CO_2 stability by much as the i3 site is the most stable with an E_{ads} of -0.219 eV and a 3.124 Å CO_2 -FM distance.

From here, we transitioned to CH_5N_3 and $\text{C}_3\text{N}_2\text{H}_4$ FMs as Lee et al.³¹ predicted favorable interactions with CO_2 , similar to that of $\text{C}_5\text{H}_5\text{N}$ (without the CO_2 -PG vdW energy contribution). CH_5N_3 is most stable (-0.530 eV and 2.611 Å FM-PG distance) on PG with C in the T site and the N atoms in the H sites (TH). CO_2 physisorbs on CH_5N_3 FG in the T site with an E_{ads} of -0.159 eV and a 2.734 Å CO_2 -FM distance. However, a N-C bond (-0.979 eV and 1.506 Å CO_2 -FM distance) was formed with CO_2 inserted next to CH_5N_3 (i3). Next, we predicted that $\text{C}_3\text{N}_2\text{H}_4$ is thermally stable on PG in the T2 site with an E_{ads} of -0.526 eV and a 3.087 Å FM-PG distance. CO_2 physisorbs on $\text{C}_3\text{N}_2\text{H}_4$ FG in the T site with an E_{ads} of -0.167 eV and a 2.883 Å CO_2 -FM distance. However, similar to CH_5N_3 , a N-C bond (-0.574 eV and 1.611 Å CO_2 -FM distance) was formed by CO_2 in the i1 site on $\text{C}_3\text{N}_2\text{H}_4$ FG. Both CH_5N_3 and $\text{C}_3\text{N}_2\text{H}_4$ showed promise being thermally stable on PG but they interact too strongly with CO_2 , indicating that Lee et al.³¹ predicted local CO_2 interaction minima with CH_5N_3 and $\text{C}_3\text{N}_2\text{H}_4$. Overall, we predicted that NH_2CH_3 and $\text{C}_5\text{H}_5\text{N}$ FG support favorable CO_2 interactions that are energetically near our target $\text{CO}_2 E_{\text{ads}}$. In addition, we predicted that $\text{C}_5\text{H}_5\text{N}$ FG is thermally stable whereas NH_2CH_3 FG is not.

Table S2. FMs E_{ads} on PG with shortest atomic distances (y (vacuum) direction or elements are in parentheses if a bond is formed) in the y direction (vacuum). Gray indicates the most stable FM site.

FM/Site	E _{ads} (eV)	vdW E _{ads} (eV)	FM-PG (Å)
CO	-0.201	-0.116	3.245
COOH	-0.402	-0.298	1.609 (C)
OH	-0.960	-0.146	1.507 (O)
NH₂T	-0.321	-0.219	1.473 (N)
NH ₂ H	-0.231	-0.103	3.036
NH ₂ B	-0.211	-0.081	3.250
NH₂CH₃T1	-0.265	-0.193	2.698
NH ₂ CH ₃ T2	-0.265	-0.178	2.777
NH ₂ CH ₃ T3	-0.264	-0.185	2.734
NH ₂ CH ₃ T4	-0.243	-0.284	2.676
NH ₂ CH ₃ H1	-0.261	-0.182	2.758
NH ₂ CH ₃ H2	-0.261	-0.180	2.770
NH ₂ CH ₃ H3	-0.246	-0.286	2.626
NH ₂ CH ₃ B1	-0.263	-0.186	2.740
NH ₂ CH ₃ B2	-0.262	-0.165	2.830
NHCH ₃ T1	-0.317	-0.407	1.518 (N)
NHCH₃T2	-0.320	-0.403	1.516 (N)
NH₂CH₂T	-0.417	-0.453	1.839 (C)
C ₅ H ₅ NT	-0.494	-0.469	3.276
C₅H₅NH	-0.543	-0.516	3.228
C ₅ H ₅ NB	-0.542	-0.464	3.266
C ₆ H ₅ NH ₂ H1	-0.607	-0.585	3.266
C₆H₅NH₂H2	-0.633	-0.625	2.937
C ₆ H ₅ NH ₂ B	-0.618	-0.586	2.810
CH ₅ N ₃ TT	-0.493	-0.389	2.770
CH₅N₃TH	-0.530	-0.440	2.611
CH ₅ N ₃ HT	-0.498	-0.408	2.727
CH ₅ N ₃ HB	-0.524	-0.386	2.886
C ₃ N ₂ H ₄ T1	-0.503	-0.438	3.029
C₃N₂H₄T2	-0.526	-0.432	3.087
C ₃ N ₂ H ₄ TT1	-0.464	-0.388	3.098
C ₃ N ₂ H ₄ TT2	-0.494	-0.369	3.207
C ₃ N ₂ H ₄ TT3	-0.438	-0.395	3.080
C ₃ N ₂ H ₄ H	-0.485	-0.455	3.003

Table S3. CO₂ E_{ads} on FG with shortest atomic distances between FM and CO₂ (elements are in parentheses if a bond is formed), CO₂ and PG (y (vacuum) direction), and FM and PG (y (vacuum) direction or elements are in parentheses if a bond is formed). Gray indicates the most stable CO₂ site.

FM/G/Site	E _{ads} (eV)	vdW E _{ads} (eV)	FM-CO ₂ (Å)	CO ₂ -PG (Å)	FM-PG (Å)
COG	-0.058	-0.038	3.260	6.554	3.231
COOHG1	-0.220	-0.074	1.911 (H-O)	4.950	1.608 (C)
COOHG2	-0.191	-0.138	2.425 (H-O)	2.810	1.608 (C)
OHGT	-0.152	-0.076	2.447	4.633	1.510 (O)
OHGi	-0.643	-0.137	1.375 (O-C)	2.883	3.461
NH ₂ GT1	-0.096	-0.082	2.634	5.056	1.475 (N)
NH ₂ GT2	-0.036	-0.056	2.913	5.341	1.474 (N)
NH₂Gi1	-0.979	-0.117	1.390 (N-C)	2.913	3.297
NH ₂ Gi2	-0.176	-0.199	3.134	3.001	1.474 (N)
NH ₂ CH ₃ GT	-0.078	-0.061	2.776	7.794	2.713
NH ₂ CH ₃ Gi1	-0.341	-0.219	2.928	3.220	2.793
NH₂CH₃Gi2	-0.367	-0.248	2.893	3.203	2.613
NH ₂ CH ₃ Gi3	-0.208	-0.168	2.942	3.219	2.616
C ₅ H ₅ NGT	-0.129	-0.126	3.192	6.391	3.199
C₅H₅NGi1	-0.347	-0.229	2.758	3.271	3.231
C ₅ H ₅ NGi2	-0.346	-0.233	2.719	3.208	3.200
C ₆ H ₅ NH ₂ GT1	-0.170	-0.140	2.888	6.088	2.780
C ₆ H ₅ NH ₂ GT2	-0.136	-0.135	2.967	6.080	2.806
C ₆ H ₅ NH ₂ Gi1	-0.218	-0.210	3.181	3.391	2.852
C ₆ H ₅ NH ₂ Gi2	-0.150	-0.031	2.945	3.200	2.923
C₆H₅NH₂Gi3	-0.219	-0.214	3.124	3.305	2.959
CH ₅ N ₃ GT	-0.159	-0.102	2.734	6.051	2.596
CH ₅ N ₃ Gi1	-0.449	-0.221	2.305	3.201	2.655
CH ₅ N ₃ Gi2	-0.450	-0.241	2.253	3.226	2.614
CH₅N₃Gi3	-0.979	-0.191	1.506 (N-C)	3.209	3.054
C ₃ N ₂ H ₄ GT	-0.167	-0.089	2.883	6.282	3.080
C₃N₂H₄Gi1	-0.574	-0.270	1.611 (N-C)	3.202	3.272
C ₃ N ₂ H ₄ Gi2	-0.571	-0.266	1.614 (N-C)	3.200	3.245

For the following figures, the odd columns are the xz plane view and the even columns are the yz plane view (unless specified otherwise). The most stable adsorption geometry is indicated by the red box.

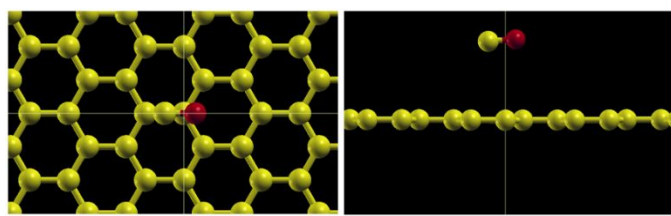


Figure S9. Ionically relaxed CO on PG.

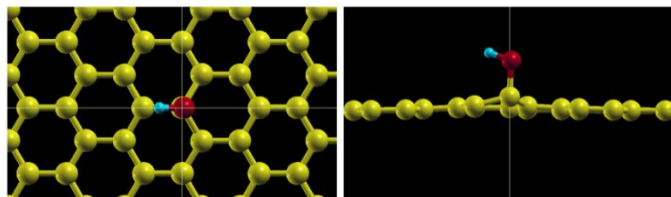


Figure S10. Ionically relaxed OH on PG.

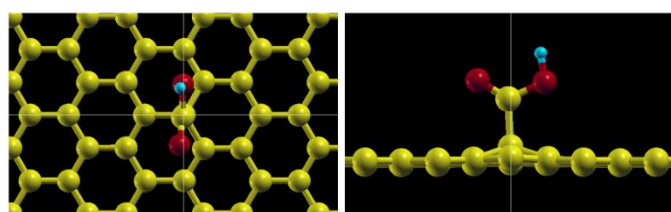


Figure S11. Ionically relaxed COOH on PG (right image is xy plane).

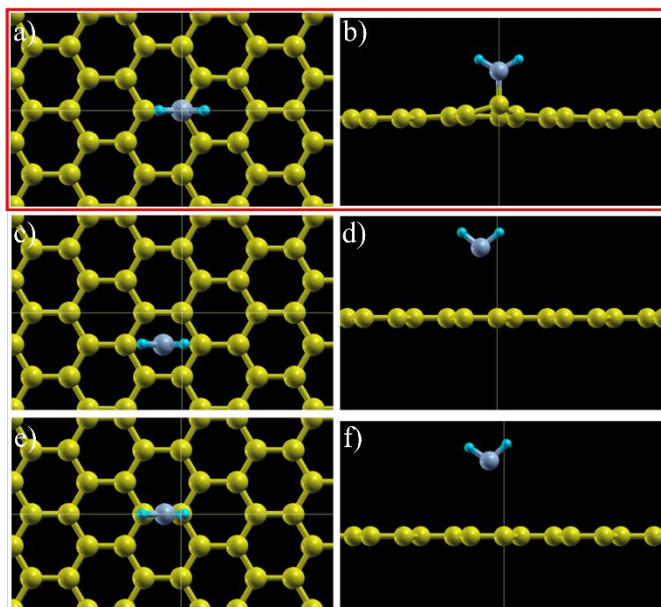


Figure S12. Ionically relaxed NH_2 configuration on PG in NH_2T (a, b), NH_2H (c, d), and NH_2B (e, f) sites.

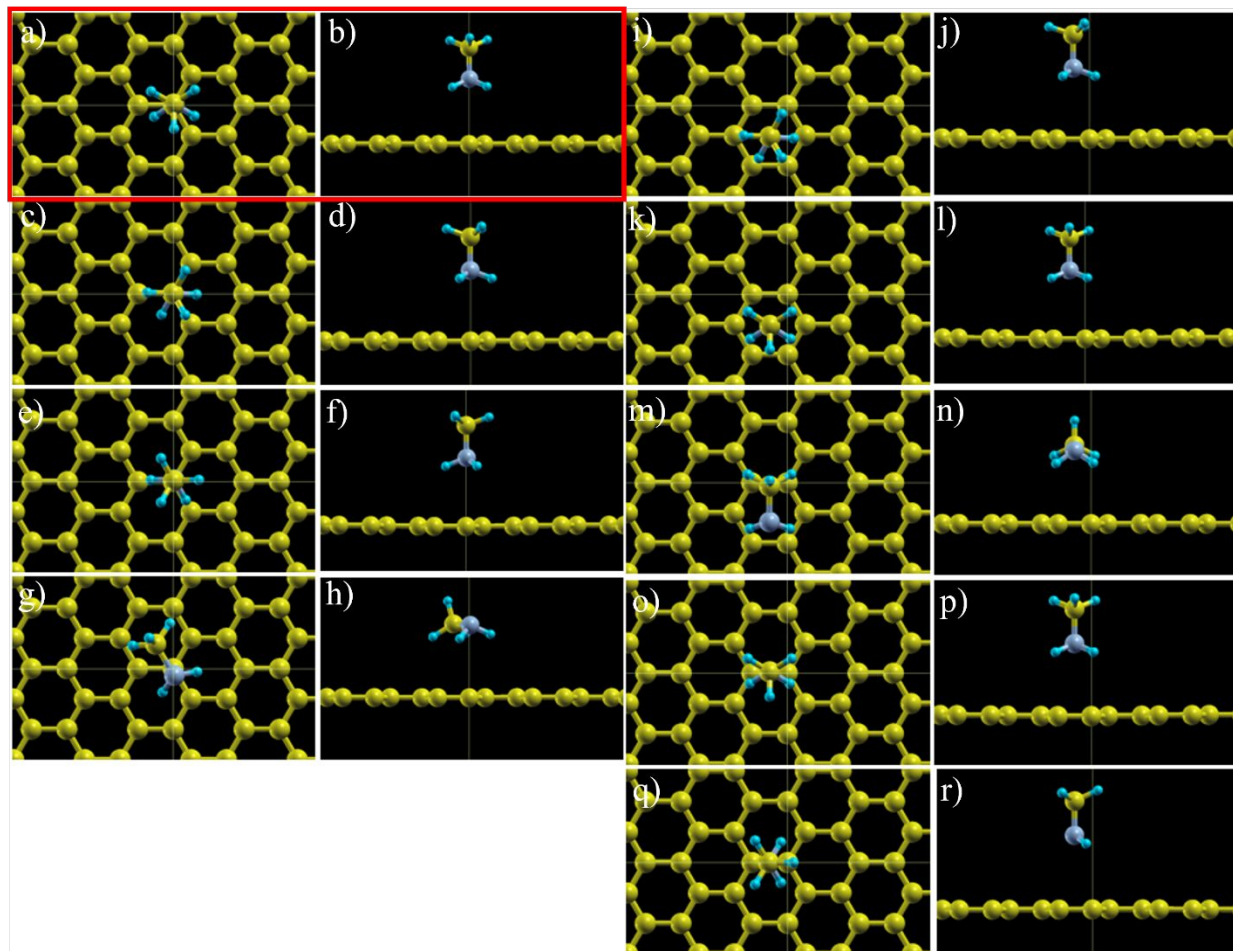


Figure S13. Ionically relaxed NH_2CH_3 configuration on PG in $\text{NH}_2\text{CH}_3\text{T}1$ (a, b), $\text{NH}_2\text{CH}_3\text{T}2$ (c, d), $\text{NH}_2\text{CH}_3\text{T}3$ (e, f), $\text{NH}_2\text{CH}_3\text{T}4$ (g, h), $\text{NH}_2\text{CH}_3\text{H}1$ (i, j), $\text{NH}_2\text{CH}_3\text{H}2$ (k, l), $\text{NH}_2\text{CH}_3\text{H}3$ (m, n), $\text{NH}_2\text{CH}_3\text{B}1$ (o, p), and $\text{NH}_2\text{CH}_3\text{B}2$ (q, r) sites.

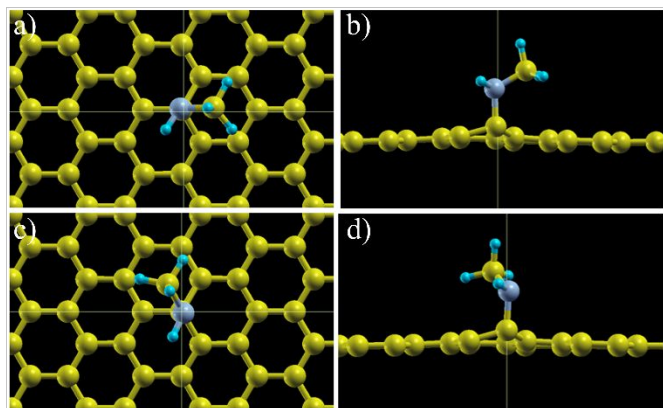


Figure S14. Ionically relaxed NHCH_3 configuration on PG in $\text{NHCH}_3\text{T}1$ (a, b) and $\text{NHCH}_3\text{T}2$ (c, d) sites.

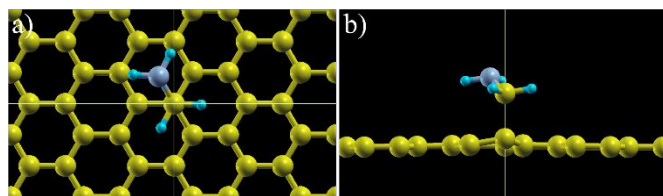


Figure S15. Ionically relaxed NH_2CH_2 configuration on PG in $\text{NH}_2\text{CH}_2\text{T}$ (a, b) site.

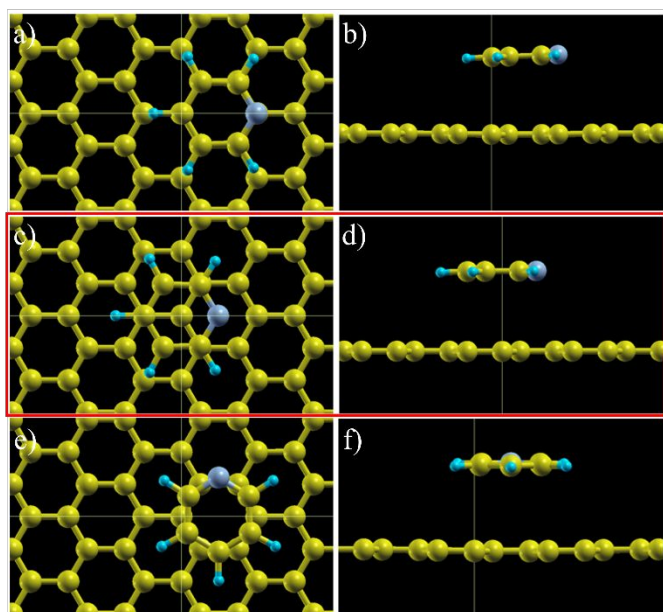


Figure S16. Ionically relaxed $\text{C}_5\text{H}_5\text{N}$ configuration on PG in $\text{C}_5\text{H}_5\text{NT}$ (a, b), $\text{C}_5\text{H}_5\text{NH}$ (c, d), and $\text{C}_5\text{H}_5\text{NB}$ (e, f) sites.

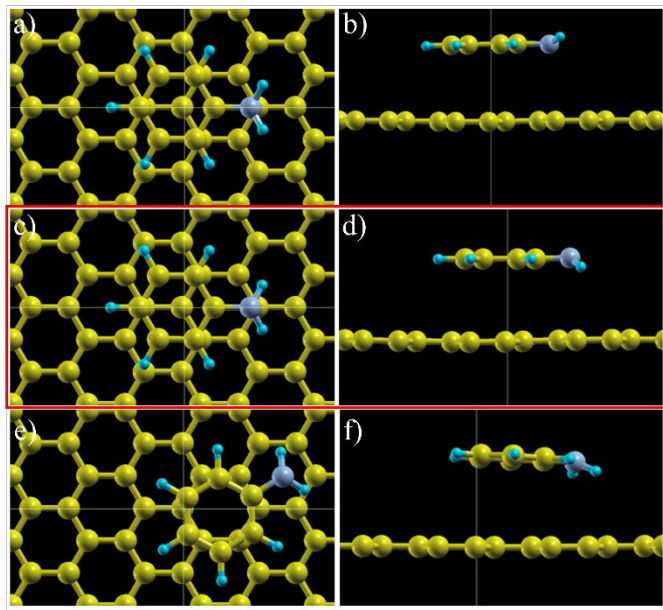


Figure S17. Ionically relaxed $\text{C}_6\text{H}_5\text{NH}_2$ configuration on PG in $\text{C}_6\text{H}_5\text{NH}_2\text{H}1$ (a, b), $\text{C}_6\text{H}_5\text{NH}_2\text{H}2$ (c, d), and $\text{C}_6\text{H}_5\text{NH}_2\text{B}$ (e, f) sites.

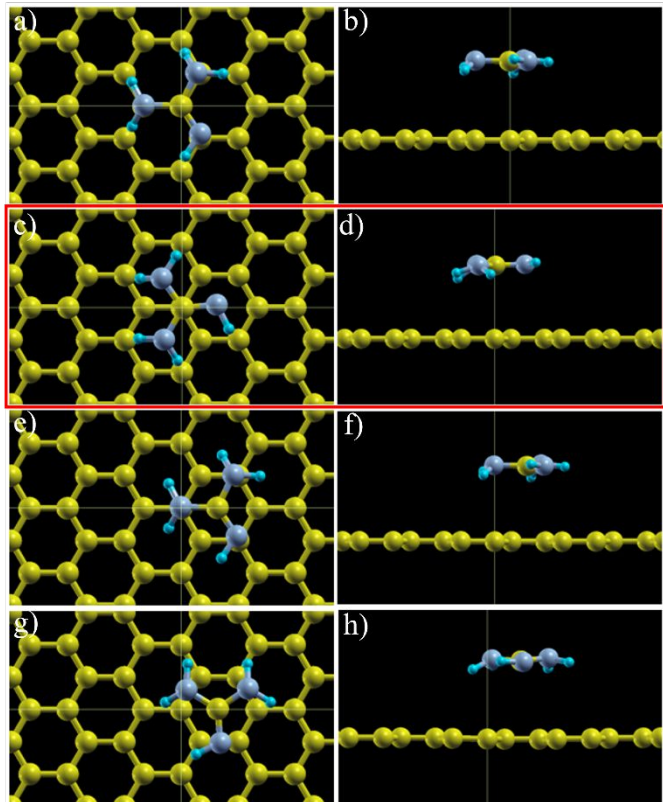


Figure S18. Ionically relaxed CH_5N_3 configuration on PG in $\text{CH}_5\text{N}_3\text{TT}$ (a, b), $\text{CH}_5\text{N}_3\text{TH}$ (c, d), $\text{CH}_5\text{N}_3\text{HT}$ (e, f), and $\text{CH}_5\text{N}_3\text{HB}$ (g, h) sites.

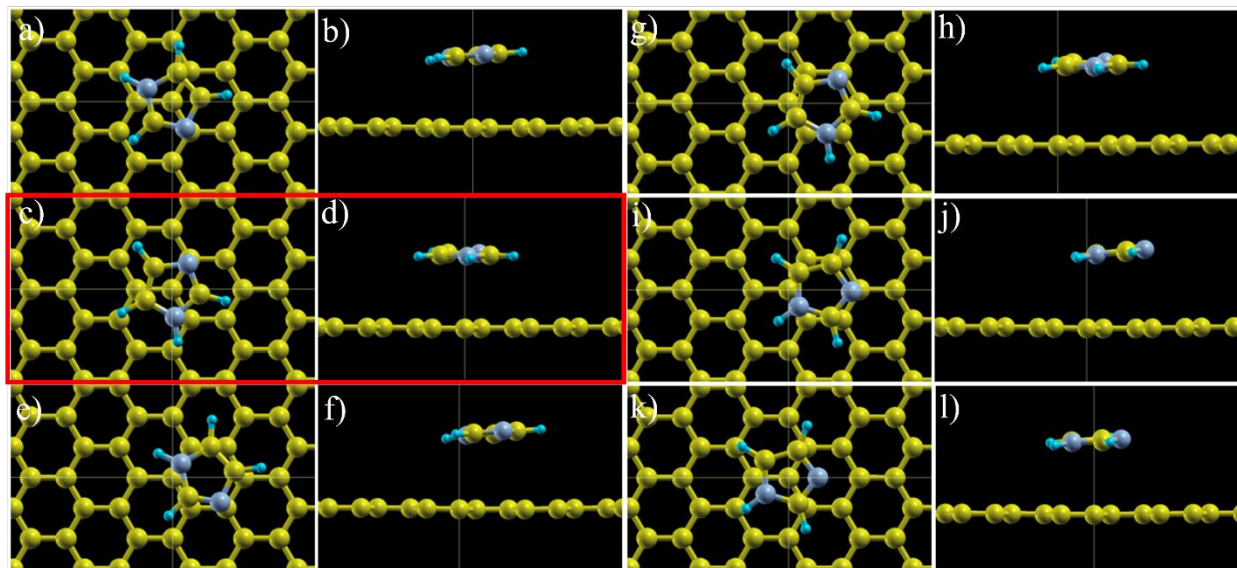


Figure S19. Ionically relaxed $\text{C}_3\text{N}_2\text{H}_4$ configuration on PG in $\text{C}_3\text{N}_2\text{H}_4\text{T}1$ (a, b), $\text{C}_3\text{N}_2\text{H}_4\text{T}2$ (c, d), $\text{C}_3\text{N}_2\text{H}_4\text{TT}1$ (e, f), $\text{C}_3\text{N}_2\text{H}_4\text{TT}2$ (g, h), $\text{C}_3\text{N}_2\text{H}_4\text{TT}3$ (i, j), and $\text{C}_3\text{N}_2\text{H}_4\text{H}$ (k, l) sites.

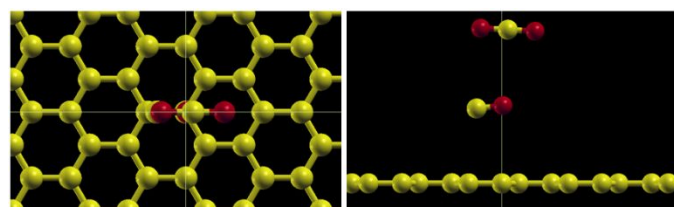


Figure S20. Ionically relaxed CO_2 configuration on COG.

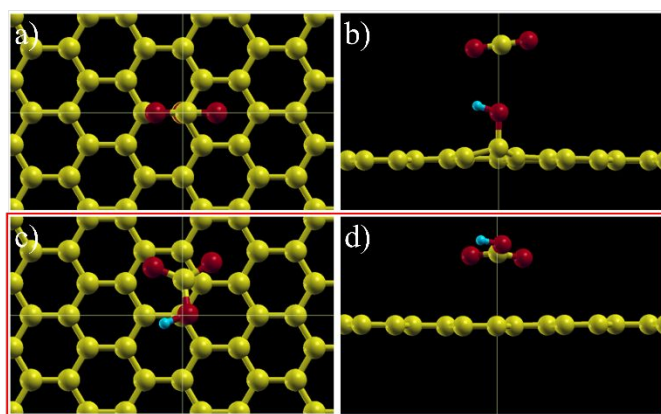


Figure S21. Ionically relaxed CO_2 configuration on OHGT (a, b) and OHGi (c, d) sites.

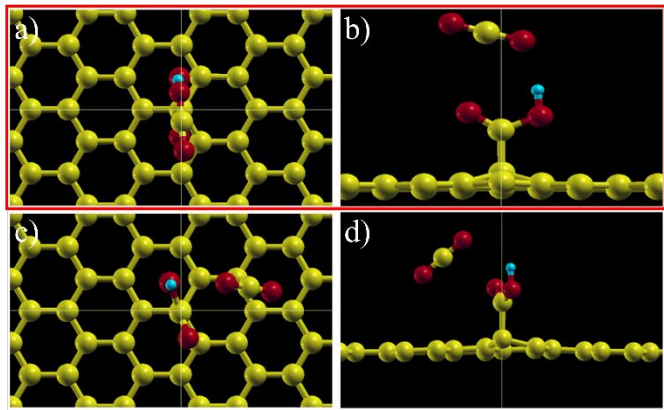


Figure S22. Ionically relaxed CO₂ configuration on COOHG1 (a, b (xy plane)) and COOHG2 (c, d) sites.

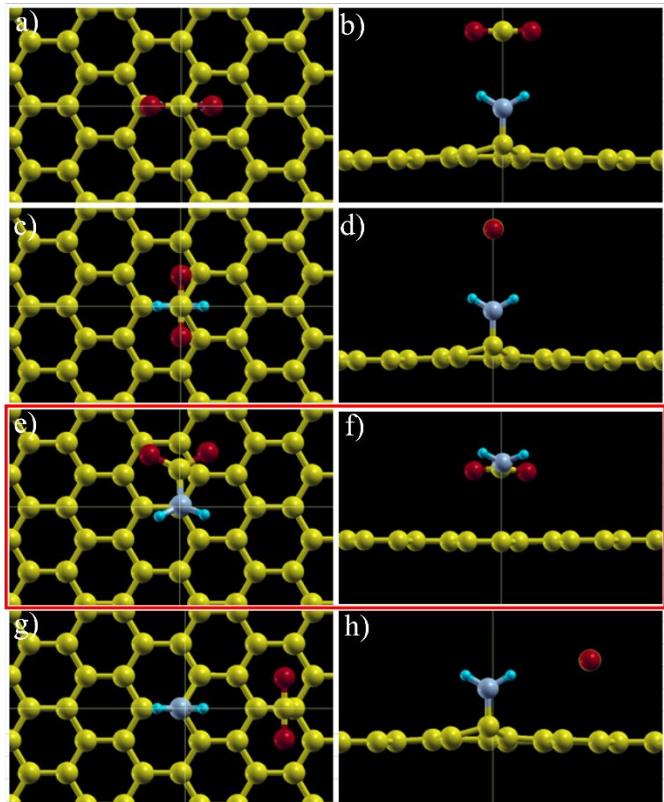


Figure S23. Ionically relaxed CO₂ configuration on NH₂GT1 (a, b), NH₂GT2 (c, d), NH₂Gi1 (e, f), and NH₂Gi2 (g, h) sites.

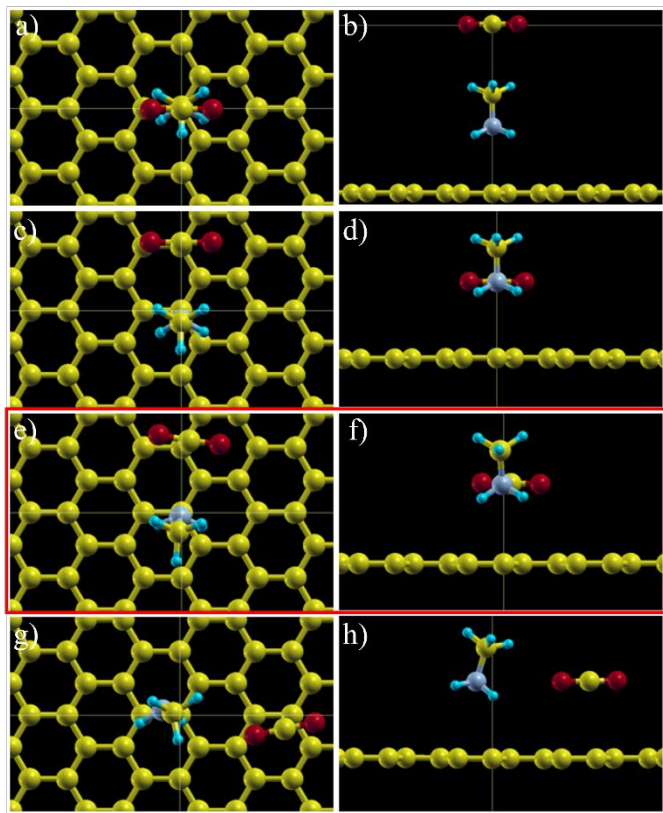


Figure S24. Ionically relaxed CO₂ configuration on NH₂CH₃GT (a, b), NH₂CH₃Gi1 (c, d), NH₂CH₃Gi2 (e, f), and NH₂CH₃Gi3 (g, h) sites.

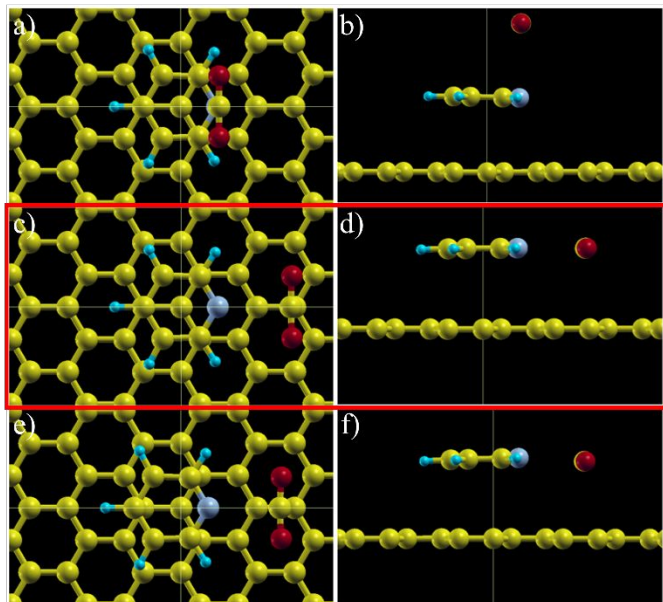


Figure S25. Ionically relaxed CO₂ configuration on C₅H₅NGT (a, b), C₅H₅NGi1 (c, d), and C₅H₅NGi2 (e, f) sites.

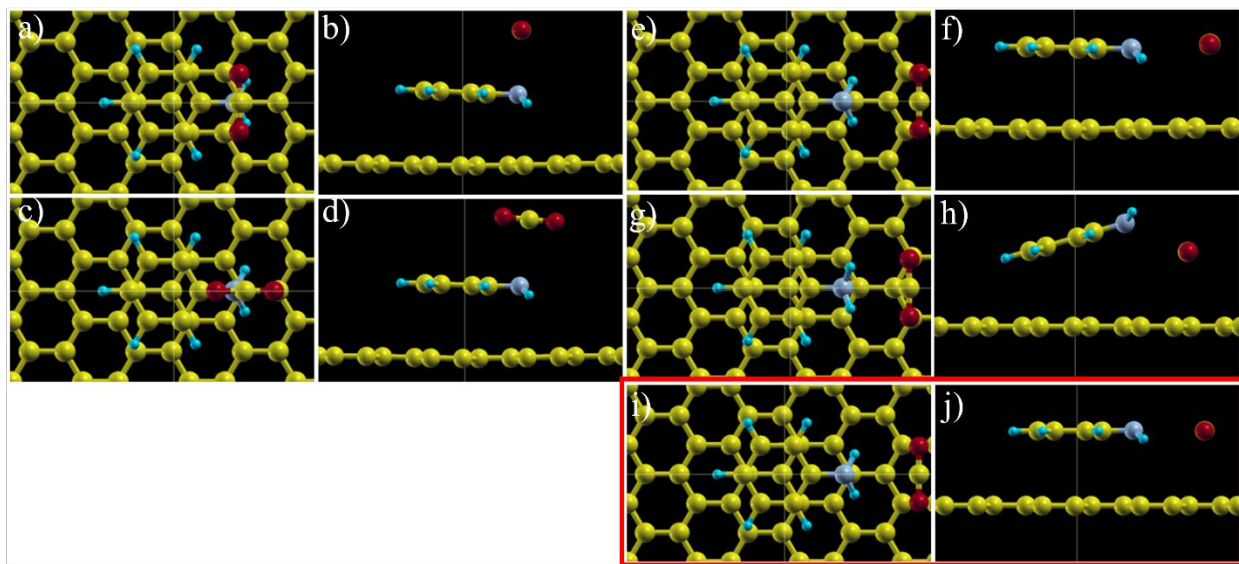


Figure S26. Ionically relaxed CO_2 configuration on $\text{C}_6\text{H}_5\text{NH}_2\text{GT1}$ (a, b), $\text{C}_6\text{H}_5\text{NH}_2\text{GT2}$ (c, d), $\text{C}_6\text{H}_5\text{NH}_2\text{Gi1}$ (e, f), $\text{C}_6\text{H}_5\text{NH}_2\text{Gi2}$ (g, h), and $\text{C}_6\text{H}_5\text{NH}_2\text{Gi3}$ (i, j) sites.

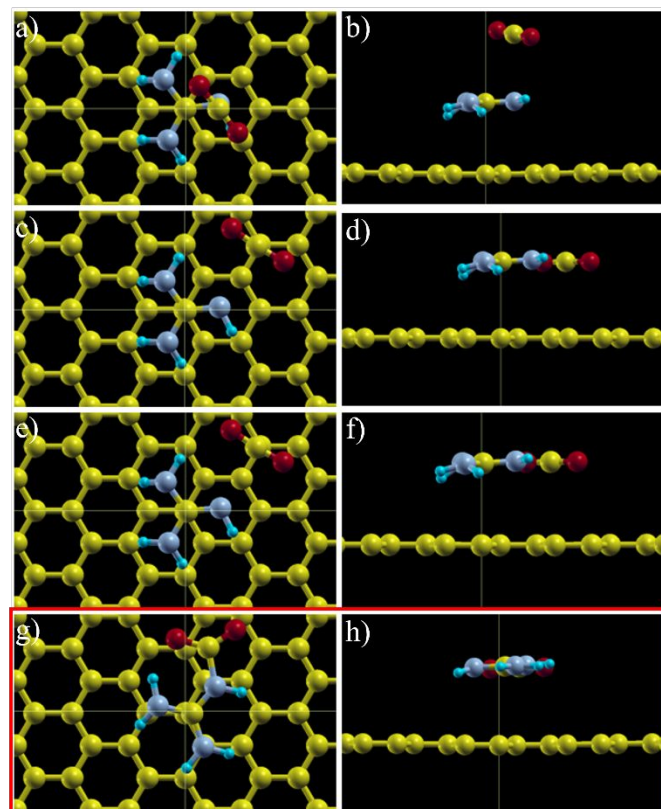


Figure S27. Ionically relaxed CO₂ configuration on CH₅N₃GT (a, b), CH₅N₃Gi1 (c, d), CH₅N₃Gi2 (e, f), and CH₅N₃Gi3 (g, h) sites.

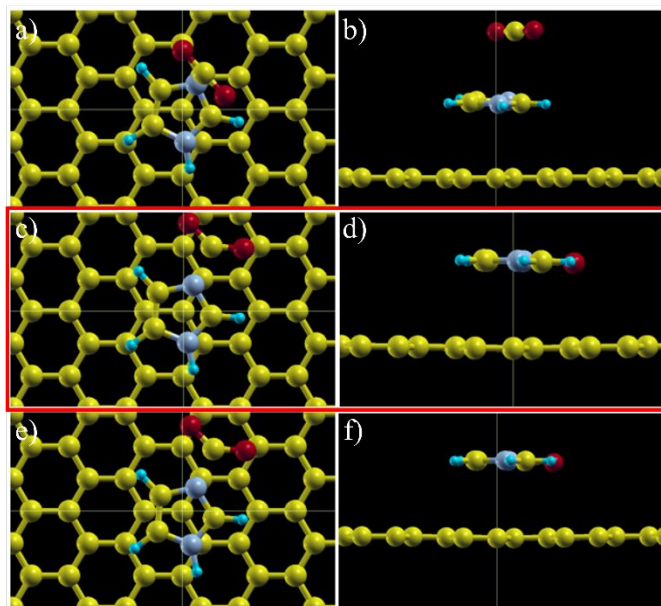


Figure S28. Ionically relaxed CO₂ configuration on C₃N₂H₄GT (a, b), C₃N₂H₄Gi1 (c, d), and C₃N₂H₄Gi2 (e, f) sites.

CO₂ Adsorption on Monovacancy Defect Graphene (MG)

We predicted the defect sensitivity of methylamine and pyridine FG by calculating CO₂ E_{ads} with defects (see Table S4 and Figures S29 and S30 for FM E_{ads} and geometry; see Table S5 and Figures S31-S33 for CO₂ E_{ads} and geometry). In this study, we only considered monovacancy defects as Wang et al.¹⁷ predicted that MG alters CO₂ E_{ads} (due to dangling bonds) greater than other common defects like Stone-Wales. For MG, CO₂ is placed in four different orientations in the defect site. The most stable site (MG4) results in a CO₂ E_{ads} of -0.370 eV and a 2.759 Å CO₂-PG distance (consistent with Wang et al.)¹⁷. MG provides an opportunity to increase CO₂ E_{ads} near our target, however, point defects are difficult to control and therefore methylamine and pyridine are checked to determine if they are sensitive to these defects. Methylamine physisorbs on MG with an E_{ads} of -0.380 eV and a 2.535 Å FM-MG distance. By including CO₂ in the i1 site, CO₂ is near our target CO₂ E_{ads} (-0.373 eV and 2.861 Å FM-CO₂ distance), similar to that of methylamine on PG. Pyridine forms two C-C bonds (1.520 Å, sp³ hybridized) in the B1 site with MG (-1.875 eV), making pyridine even more thermally stable than on PG. However, pyridine is near perpendicular to MG, which results in a less stable CO₂ E_{ads} (-0.258 eV, i3), when compared to CO₂ interacting with pyridine on PG (see Table S3). Overall, methylamine is defect insensitive whereas pyridine is defect sensitive.

Table S4. FMs E_{ads} on MG with shortest atomic distances (y (vacuum) direction or elements are in parentheses if a bond is formed). Gray indicates the most stable FM site.

Material/G/Site	E _{ads} (eV)	vdW E _{ads} (eV)	FM-MG (Å)
NH₂CH₃MG1	-0.380	-0.191	2.535
NH ₂ CH ₃ MG2	-0.339	-0.196	2.713
C ₅ H ₅ NMGT1	-0.552	-0.436	3.202
C ₅ H ₅ NMGT2	-0.405	-0.432	3.265
C ₅ H ₅ NMGH	-0.548	-0.476	2.995
C₅H₅NMGB1	-1.875	-0.713	1.520 (C)
C ₅ H ₅ NMGB2	-0.886	-0.750	1.504 (C)
C ₅ H ₅ NMGB3	-1.801	-0.741	1.518 (C)

Table S5. CO₂ E_{ads} on FG on MG with shortest atomic distances between FM and CO₂ (elements are in parentheses if a bond is formed), CO₂ and PG (y (vacuum) direction), and FM and PG (y (vacuum) direction or elements are in parentheses if a bond is formed). Gray indicates the most stable CO₂ site while * indicates unstable sites.

Material/G/Site	E _{ads} (eV)	vdW E _{ads} (eV)	FM-CO ₂ (Å)	CO ₂ -PG (Å)	FM-PG (Å)
MG1	-0.243	-0.180	-	2.763	-
MG2	-0.268	-0.179	-	2.768	-
MG3	-0.159	-0.186	-	2.826	-
MG4	-0.370	-0.183	-	2.759	-
MGNH₂CH₃i1	-0.373	-0.237	2.861	3.219	2.442
MGNH ₂ CH ₃ i2	-0.196	-0.214	2.898	3.172	2.790
MGC ₅ H ₅ NT1	-0.205	-0.148	2.678	4.463	1.521 (C)
MGC ₅ H ₅ NT2*	0.227	-0.221	1.388 (N-C)	4.008	1.522 (C)
MGC ₅ H ₅ Ni1	-0.060	-0.333	1.698 (N-C)	2.830	1.527 (C)
MGC ₅ H ₅ Ni2	-0.062	-0.328	1.714 (N-C)	2.842	1.526 (C)
MGC₅H₅Ni3	-0.258	-0.266	2.787	3.201	1.519 (C)

For the following figures, the odd columns are the xz plane view and the even columns are the yz plane view (unless specified otherwise). The most stable adsorption geometry is indicated by the red box.

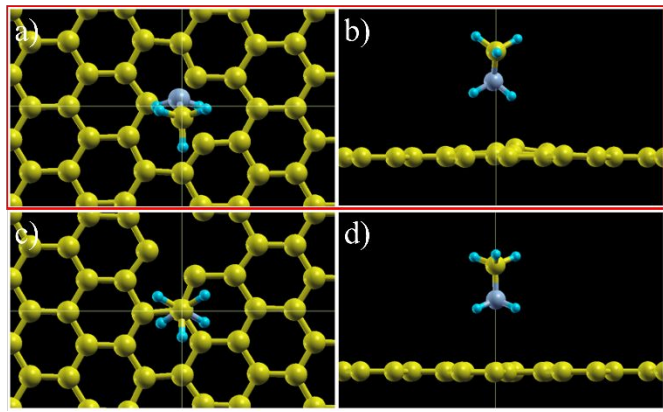


Figure S29. Ionically relaxed NH_2CH_3 configuration on MG in $\text{NH}_2\text{CH}_3\text{MG1}$ (a, b) and $\text{NH}_2\text{CH}_3\text{MG2}$ (c, d) sites.

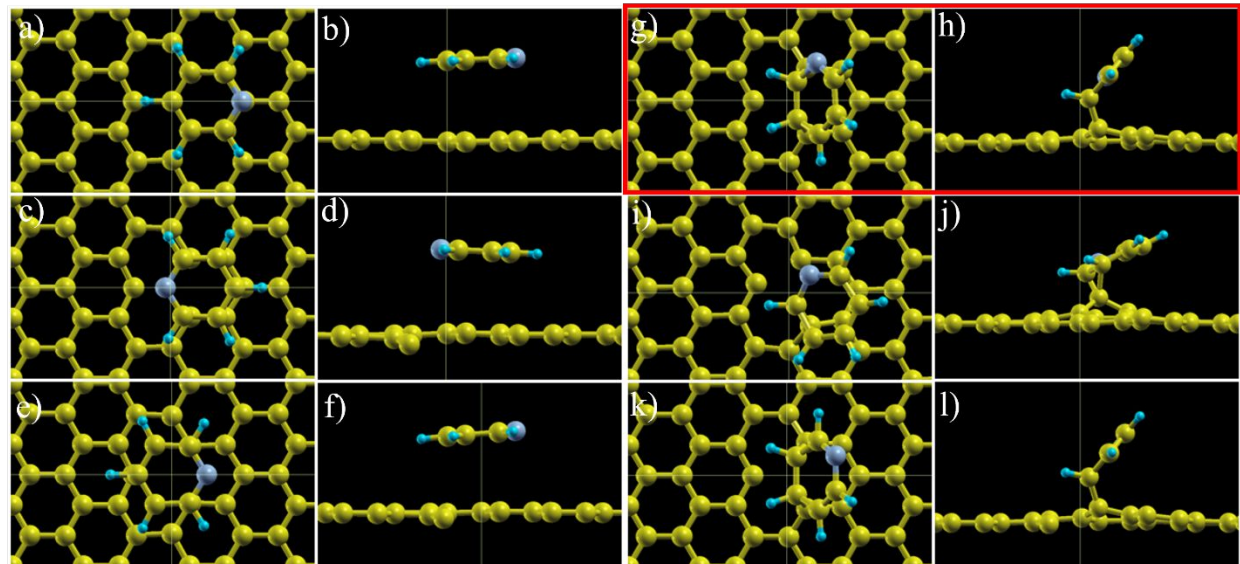


Figure S30. Ionically relaxed $\text{C}_5\text{H}_5\text{N}$ configuration on MG in $\text{C}_5\text{H}_5\text{NMGT1}$ (a, b), $\text{C}_5\text{H}_5\text{NMGT2}$ (c, d), $\text{C}_5\text{H}_5\text{NMGH}$ (e, f), $\text{C}_5\text{H}_5\text{NMGB1}$ (g, h), $\text{C}_5\text{H}_5\text{NMGB2}$ (i, j), and $\text{C}_5\text{H}_5\text{NMGB3}$ (k, l) sites.

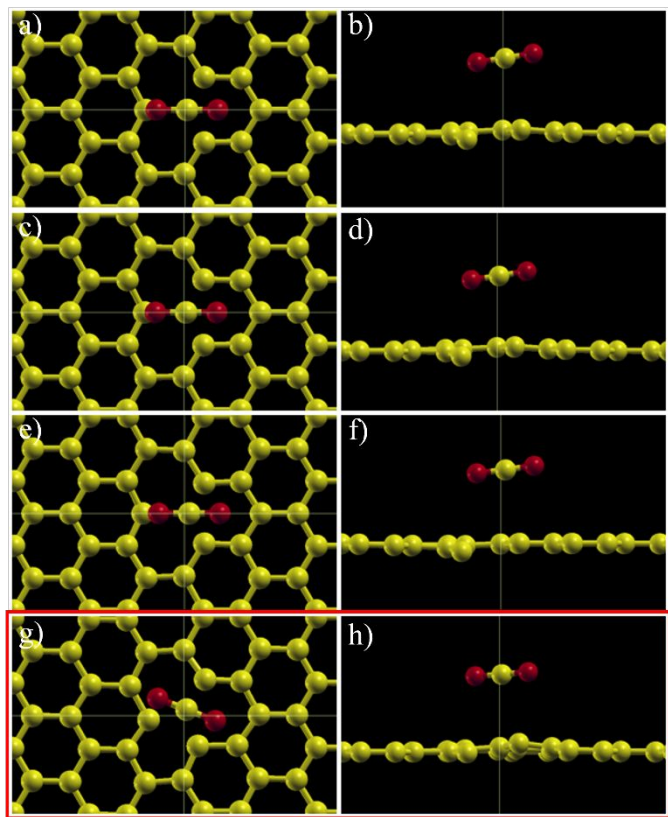


Figure S31. Ionically relaxed CO₂ configuration on MG1 (a, b), MG2 (c, d), MG3 (e, f), and MG4 (g, h) sites.

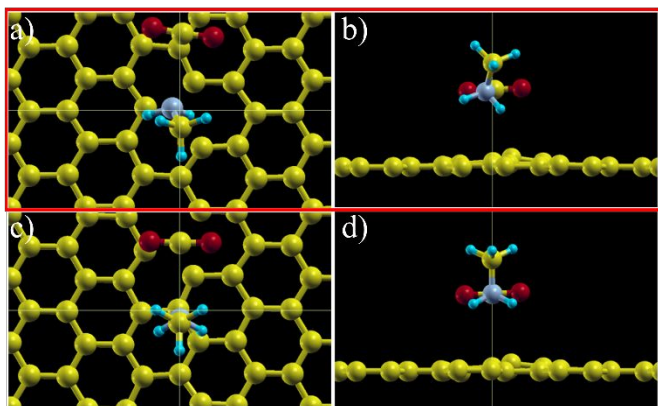


Figure S32. Ionically relaxed CO₂ configuration on MG1NH₂CH₃ (a, b) and MG2NH₂CH₃ (c, d) sites.

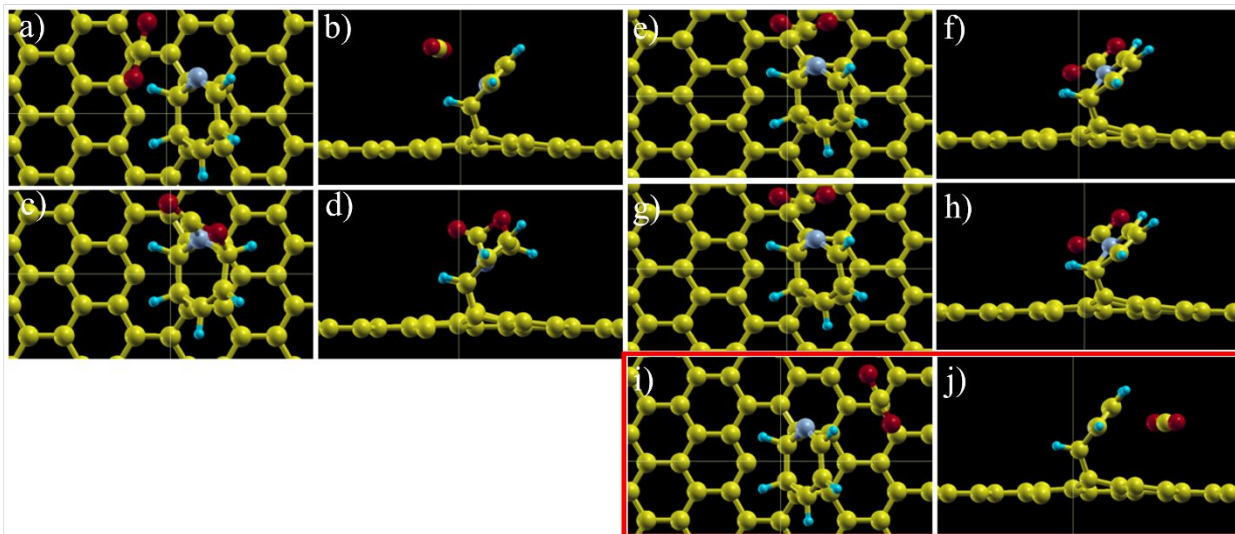


Figure S33. Ionically relaxed CO_2 configuration on $\text{MGC}_5\text{H}_5\text{NT1}$ (a, b), $\text{MGC}_5\text{H}_5\text{NT2}^*$ (c, d), $\text{MGC}_5\text{H}_5\text{Ni1}$ (e, f), $\text{MGC}_5\text{H}_5\text{Ni2}$ (g, h), and $\text{MGC}_5\text{H}_5\text{Ni3}$ (i, j) sites.

Selectivity with E_{ads}

While selectivity will be dependent on sticking coefficient, kinetic diameter, and pore size of the material in the realistic carbon capture setting, the comparative E_{ads} of CO_2 is a necessary parameter to investigate at the DFT level (see Table S6 and Figures S34-S42). H_2O , O_2 , and N_2 all physisorb on PG (see Figures S34, S37, and S40) and are most stable in the H site with E_{ads} of -0.188, -0.206, and -0.208 eV, respectively. PG energetically favors CO_2 (-0.250 eV) over H_2O , O_2 , and N_2 , but is most competitive with O_2 and N_2 . However, O_2 and N_2 prefer to adsorb onto PG rather than methylamine and pyridine FG (see Table S6), leaving the i sites open for CO_2 . Nevertheless, H_2O is more stable than CO_2 on methylamine and pyridine FG due to N-H bonding in the i1 sites (see Figures S35 and S36). H_2O forms a N-H bond with both methylamine and pyridine with E_{ads} of -0.557 eV and -0.482 eV, respectively.

Table S6. N_2 , O_2 , and H_2O E_{ads} on FG with shortest atomic distances between FM and gas (elements are in parentheses if a bond is formed), gas and PG (y (vacuum) direction), and FM and PG (y (vacuum) direction or elements are in parentheses if a bond is formed). Gray indicates the most stable gas molecule site while * indicates unstable sites.

Gas/G/FM/Site	E_{ads} (eV)	vdW (eV)	E_{ads}	FM-Gas (\AA)	Gas-PG (\AA)	FM-PG (\AA)
H_2OGT	-0.175	-0.077	-	3.144	-	
H_2OGH	-0.188	-0.082	-	3.072	-	
H_2OGB	-0.178	-0.077	-	3.143	-	
$\text{H}_2\text{OGNH}_2\text{CH}_3\text{T}$	-0.052	-0.020	2.859	7.880	2.732	

H₂OGNH₂CH₃i1	-0.557	-0.115	1.823 (N-H)	3.275	2.677
H ₂ OGNH ₂ CH ₃ i2	-0.490	-0.142	1.843 (N-H)	2.544	2.598
H ₂ OGC ₅ H ₅ NT1	-0.284	0.025	1.846 (N-H)	4.885	2.817
H ₂ OGC ₅ H ₅ NT2	-0.479	-0.149	1.829 (N-H)	3.190	3.238
H₂OGC₅H₅Ni1	-0.482	-0.147	1.826 (N-H)	3.011	3.221
H ₂ OGC ₅ H ₅ Ni2	-0.462	-0.147	1.851 (N-H)	2.556	3.261
O ₂ GT	-0.195	-0.105	-	3.077	-
O₂GH	-0.206	-0.116	-	3.027	-
O ₂ GB	-0.191	-0.110	-	3.072	-
O ₂ GNH ₂ CH ₃ T	-0.054	-0.016	2.936	7.974	2.770
O ₂ GNH ₂ CH ₃ i1	-0.088	-0.117	3.476	3.186	2.719
O₂GNH₂CH₃i2	-0.156	-0.110	2.600	3.168	2.752
O ₂ GC ₅ H ₅ NT1	-0.058	-0.030	2.954	6.340	3.161
O ₂ GC ₅ H ₅ NT2*	2.451	-0.062	1.469 (C-O)	5.063	2.894
O ₂ GC ₅ H ₅ Ni1*	0.172	0.192	2.723	2.943	4.647
O₂GC₅H₅Ni2	-0.146	-0.102	2.553	3.163	3.198
N ₂ GT1	-0.199	-0.121	-	3.189	-
N ₂ GT2	-0.168	-0.081	-	3.260	-
N₂GH1	-0.208	-0.135	-	3.163	-
N ₂ GH2	-0.179	-0.097	-	3.083	-
N ₂ GB	-0.203	-0.123	-	3.245	-
N ₂ GNH ₂ CH ₃ T	-0.051	-0.049	2.919	7.881	2.690
N₂GNH₂CH₃i1	-0.189	-0.159	3.114	3.330	2.591
N ₂ GNH ₂ CH ₃ i2	-0.151	-0.128	2.875	3.188	2.776
N ₂ GC ₅ H ₅ NT1	-0.063	-0.051	3.137	6.331	3.064
N ₂ GC ₅ H ₅ NT2	-0.083	-0.090	3.267	6.471	3.134
N ₂ GC ₅ H ₅ Ni1*	0.186	0.209	2.775	3.108	4.820
N₂GC₅H₅Ni2	-0.174	-0.118	2.657	3.309	3.201

For the following figures, the odd columns are the xz plane view and the even columns are the yz plane view (unless specified otherwise). The most stable adsorption geometry is indicated by the red box.

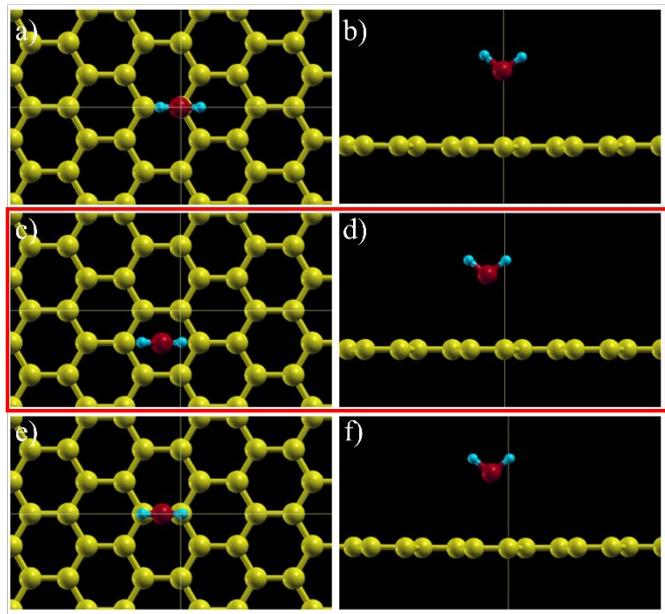


Figure S34. Ionically relaxed H_2O configuration on PG in H_2OGT (a, b), H_2OGH (c, d), and H_2OGB (e, f) sites.

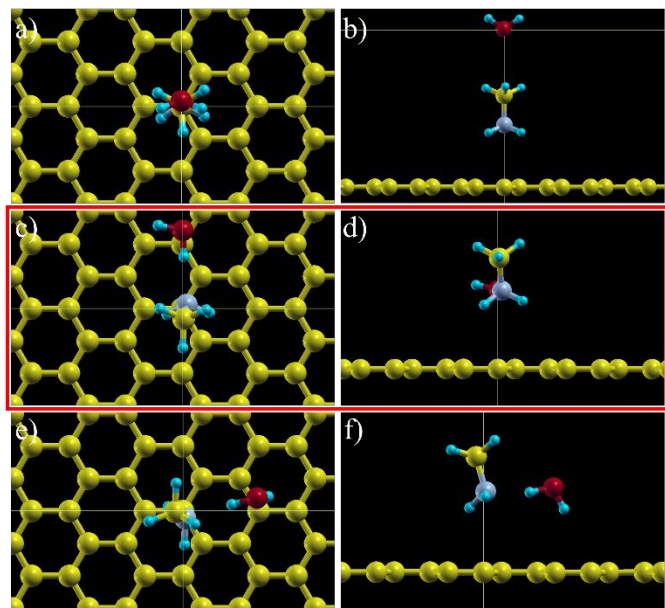


Figure S35. Ionically relaxed H_2O configuration on GNH_2CH_3 in $\text{H}_2\text{OGNH}_2\text{CH}_3\text{T}$ (a, b), $\text{H}_2\text{OGNH}_2\text{CH}_3\text{i1}$ (c, d), and $\text{H}_2\text{OGNH}_2\text{CH}_3\text{i2}$ (e, f) sites.

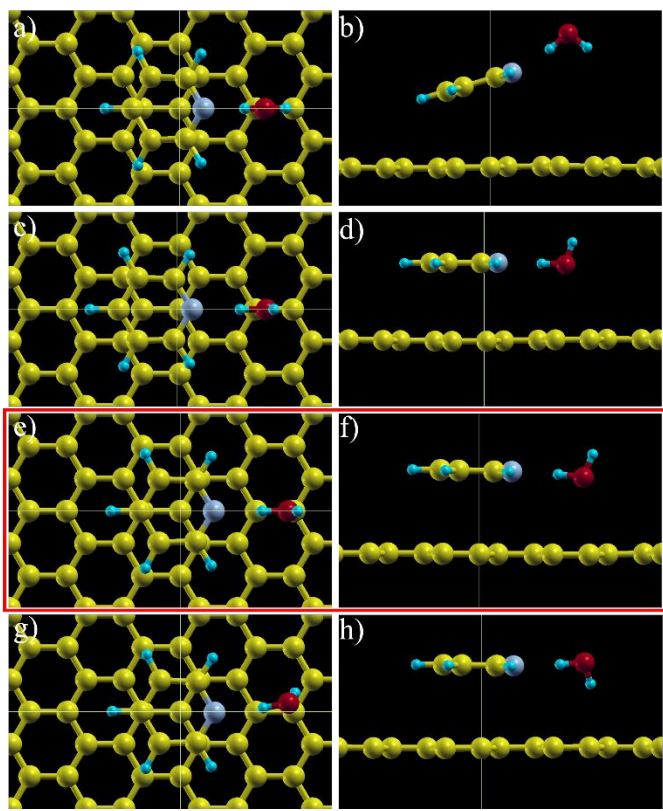


Figure S36. Ionically relaxed H_2O configuration on $\text{GC}_5\text{H}_5\text{N}$ in $\text{H}_2\text{OGC}_5\text{H}_5\text{NT1}$ (a, b), $\text{H}_2\text{OGC}_5\text{H}_5\text{NT1}$ (c, d), $\text{H}_2\text{OGC}_5\text{H}_5\text{Ni1}$ (e, f), and $\text{H}_2\text{OGC}_5\text{H}_5\text{Ni2}$ (g, h) sites.

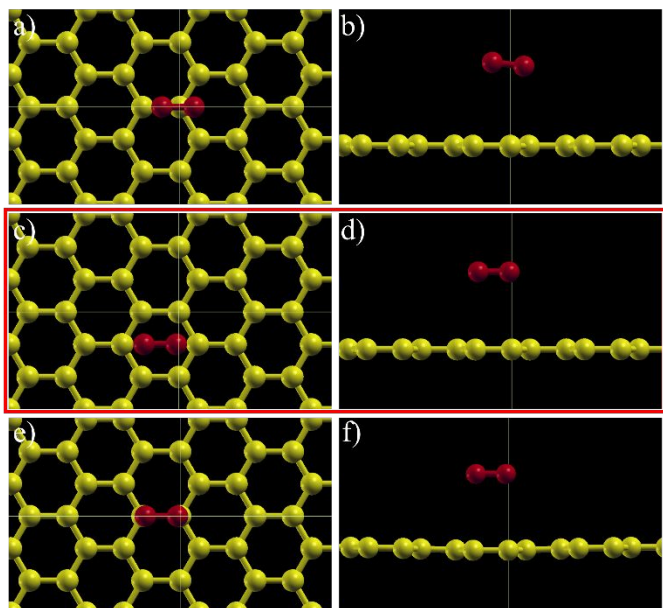


Figure S37. Ionically relaxed O_2 configuration on PG in O_2GT (a, b), O_2GH (c, d), and O_2GB (e, f) sites.

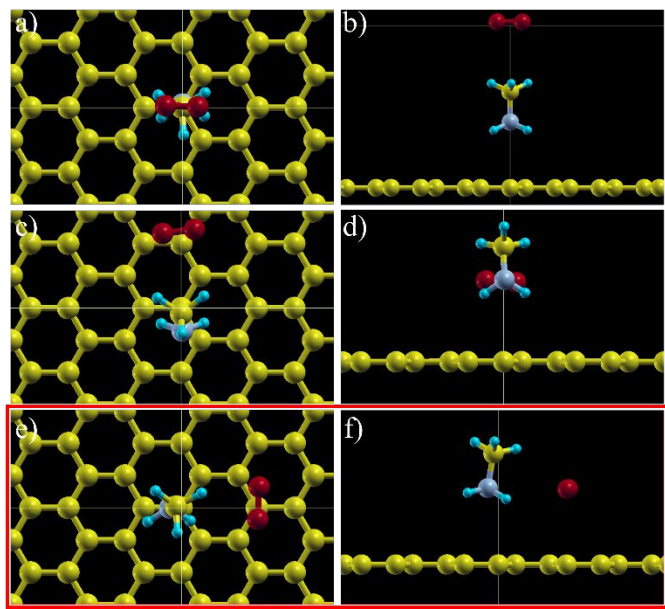


Figure S38. Ionically relaxed O_2 configuration on GNH_2CH_3 in $\text{O}_2\text{GNH}_2\text{CH}_3\text{T}$ (a, b), $\text{O}_2\text{GNH}_2\text{CH}_3\text{i1}$ (c, d), and $\text{O}_2\text{GNH}_2\text{CH}_3\text{i2}$ (e, f) sites.

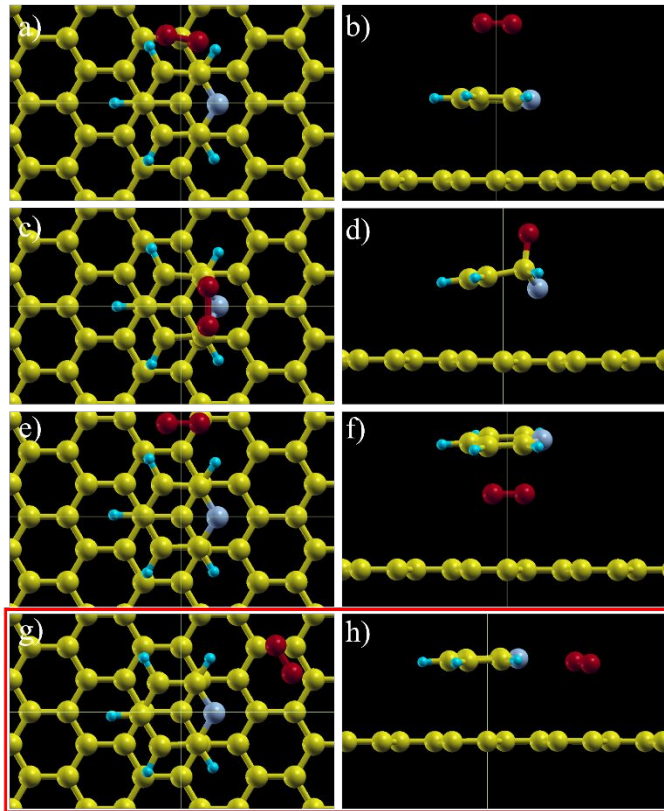


Figure S39. Ionically relaxed O₂ configuration on GC₅H₅N in O₂GC₅H₅NT1 (a, b), O₂GC₅H₅NT2* (c, d), O₂GC₅H₅Ni1* (e, f), and O₂GC₅H₅Ni2 (g, h) sites. * indicates stability.

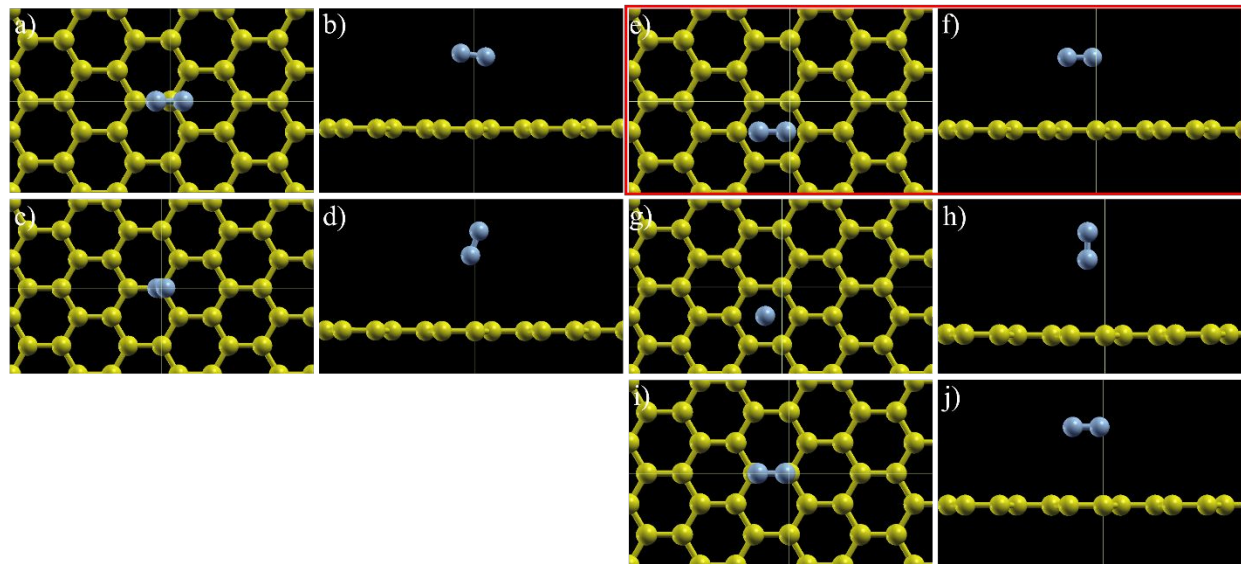


Figure S40. Ionically relaxed N₂ configuration on PG in N₂GT1 (a, b), N₂GT2 (c, d), N₂GH1 (e, f), N₂GH2 (g, h), and N₂GB (i, j) sites.

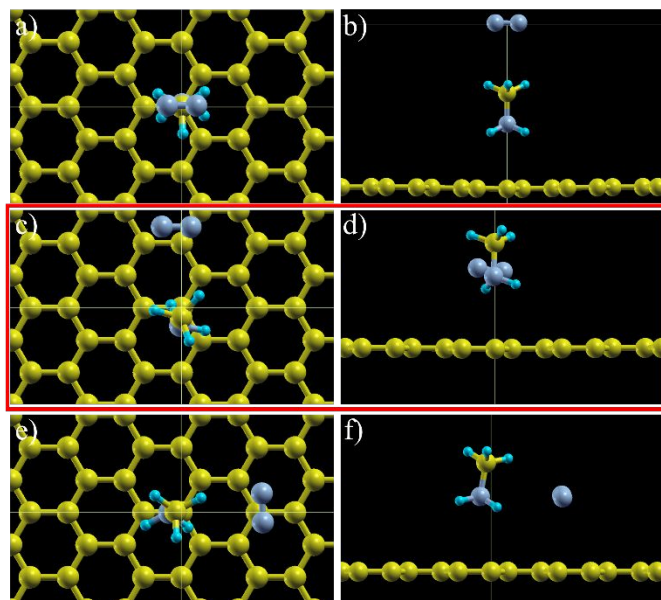


Figure S41. Ionically relaxed N₂ configuration on GNH₂CH₃ in N₂GNH₂CH₃T (a, b), N₂GNH₂CH₃i1 (c, d), and N₂GNH₂CH₃i2 (e, f) sites.

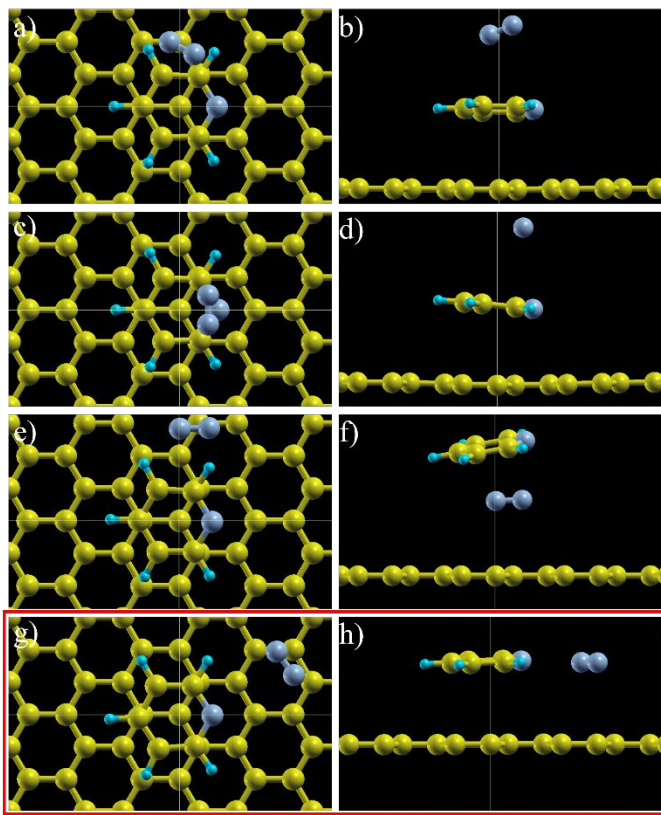


Figure S42. Ionically relaxed N_2 configuration on $\text{GC}_5\text{H}_5\text{N}$ in $\text{N}_2\text{GC}_5\text{H}_5\text{NT1}$ (a, b), $\text{N}_2\text{GC}_5\text{H}_5\text{NT1}$ (c, d), $\text{N}_2\text{GC}_5\text{H}_5\text{Ni1}^*$ (e, f), and $\text{N}_2\text{GC}_5\text{H}_5\text{Ni2}$ (g, h) sites. * indicates stability.

Coadsorption with E_{ads}

Pyridine and methylamine FG energetically favor H_2O over CO_2 , which opens the door for either cooperative or competitive adsorption (see Table S7 and Figures S43-S45). For methylamine FG, CO_2 forms carbonic acid with H_2O , which then dissociates H to NH_2CH_3 and forms NH_3CH_3^+ and bicarbonate (see Figure S43). The $\text{CO}_2 E_{\text{ads}}$ on H_2O adsorbed methylamine FG is -0.472 eV, while the bicarbonate E_{ads} on NH_3CH_3^+ FG is -0.892 eV. However, both bicarbonate and NH_3CH_3^+ will desorb together as their E_{ads} on PG is the least stable (-0.465 eV). For pyridine FG, CO_2 physisorbs to $\text{H}_2\text{OGC}_5\text{H}_5\text{N}$ with an E_{ads} of -0.282 eV and fails to form carbonic acid or bicarbonate with H_2O (see Figure S44). However, carbonic acid's E_{ads} is -0.943 eV on pyridine FG (see Figure S45) due to N-H bond (1.577 Å). Similar to methylamine FG, pyridine and carbonic acid will desorb together as their E_{ads} on PG (-0.771 eV) is less than carbonic acid separating from pyridine FG. Altogether, both methylamine and pyridine FG support cooperative adsorption with H_2O and CO_2 , and both FMs desorb with bicarbonate and carbonic acid, respectively.

Table S7. $\text{CO}_2 E_{\text{ads}}$ on H_2O adsorbed FG with shortest atomic distances between FM and gas (elements are in parentheses if a bond is formed), gas and PG (y (vacuum) direction), and FM and

PG (y (vacuum) direction or elements are in parentheses if a bond is formed). Gray indicates the most stable gas molecule site while * indicates unstable sites.

X:Y/G/FM/Site	E_{ads} (eV)	vdW E_{ads} (eV)	H_2O-CO_2 (Å)	FM- CO_2 (Å)	FM- H_2O (Å)	CO_2 - PG (Å)	H_2O - PG (Å)	FM- PG (Å)
CO₂:H₂OGNH₂CH₃i	-0.472	-0.283						
HCO ₃ GNH ₃ CH ₃	-0.892	-0.262	1.434 (O-C)	1.650 (H-O)	2.113	3.136	3.023	2.922
HCO ₃ NH ₃ CH ₃ G	-0.465	-0.422						
CO ₂ :H ₂ OGC ₅ H ₅ NT	-0.201	-0.093	2.724	3.758	1.797 (N-H)	5.794	2.517	3.200
CO₂:H₂OGC₅H₅Ni1	-0.282	-0.116	2.772	5.158	1.841 (N-H)	3.404	2.379	3.279
CO ₂ :H ₂ OGC ₅ H ₅ Ni2	-0.275	-0.097	2.760	5.221	1.841 (N-H)	3.632	2.395	3.242
CO ₂ :H ₂ OGC ₅ H ₅ Ni3	-0.253	-0.107	2.740	4.575	1.825 (N-H)	4.098	2.446	3.231
CO ₂ :H ₂ OGC ₅ H ₅ Ni4	-0.239	-0.089	2.711	4.510	1.831 (N-H)	4.410	2.419	3.241
H₂CO₃GC₅H₅Ni	-0.943	-0.352			1.577 (N-H)	-	3.131	3.263
H ₂ CO ₃ C ₅ H ₅ NG	-0.771	-0.765						

For the following figures, the odd columns are the xz plane view and the even columns are the yz plane view (unless specified otherwise). The most stable adsorption geometry is indicated by the red box.

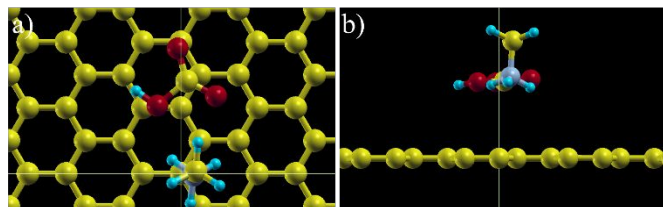


Figure S43. Ionically relaxed CO₂ configuration on H₂OGNH₂CH₃ in CO₂:H₂OGNH₂CH₃i (a, b) site.

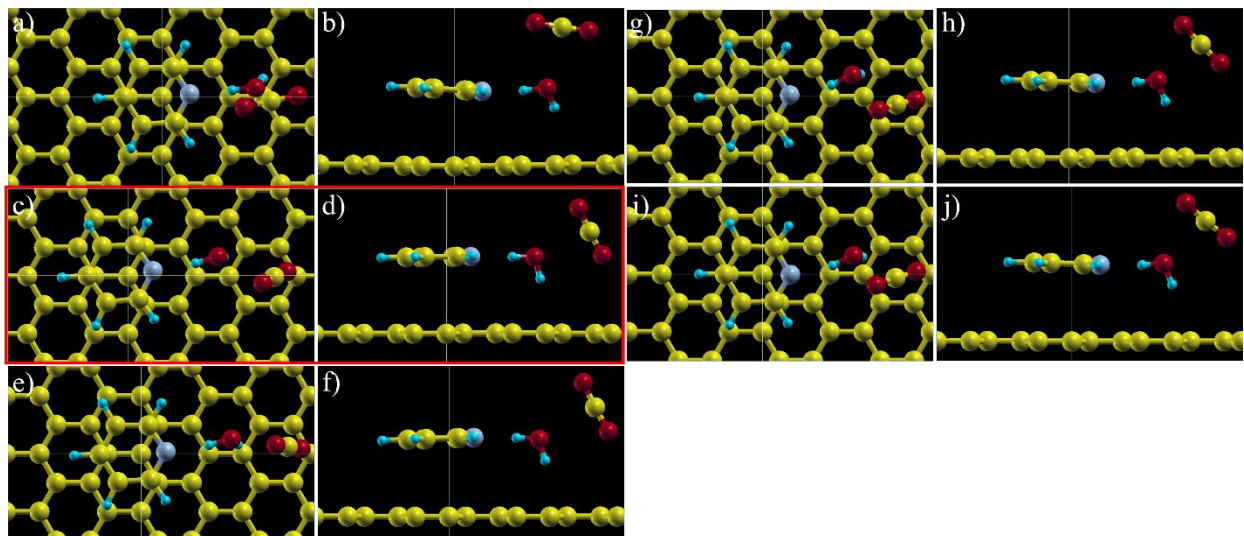


Figure S44. Ionically relaxed CO_2 configuration on $\text{H}_2\text{OGC}_5\text{H}_5\text{N}$ in $\text{CO}_2:\text{H}_2\text{OGC}_5\text{H}_5\text{NT}$ (a, b), $\text{CO}_2:\text{H}_2\text{OGC}_5\text{H}_5\text{Ni}1$ (c, d), $\text{CO}_2:\text{H}_2\text{OGC}_5\text{H}_5\text{Ni}2$ (e, f), $\text{CO}_2:\text{H}_2\text{OGC}_5\text{H}_5\text{Ni}3$ (g, h), and $\text{CO}_2:\text{H}_2\text{OGC}_5\text{H}_5\text{Ni}4$ (i, j) sites.

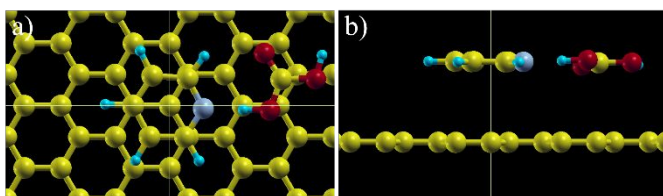


Figure S45. Ionically relaxed H_2CO_3 configuration on $\text{GC}_5\text{H}_5\text{N}$ in $\text{H}_2\text{CO}_3\text{GC}_5\text{H}_5\text{Ni}$ (a, b) site.

Coverage Effects on $\text{CO}_2 E_{\text{ads}}$

Coverage of CO_2 on graphene ceases to play a significant role according to $\text{CO}_2 E_{\text{ads}}$. To procure this discovery, we used the Langmuir Isotherm^{32,33} model to predict CO_2 coverage at select CO_2 concentrations (see equation S1).

$$\theta = \frac{KP}{1+KP} \quad (\text{S1})$$

Where θ is coverage (CO_2 molecules/C atom), K is the Langmuir constant (1.12 bar^{-1} for CO_2)³⁴, and P is partial pressure of the gas (bar). At 400 ppm, CO_2 has a graphene surface coverage of $1.60 \times 10^{-18} \text{ g}/\text{CO}_2 \text{ molecule}$,³⁴ which is $\sim 2211 \text{ C atoms}/\text{CO}_2 \text{ molecule}$ for PG. The computational limit for standard plane-wave DFT code is around a couple hundred atoms. We

incrementally calculated CO₂ E_{ads} on PG in sheets of 36, 252, 780, and 1152 C atoms, which required the use of real-space DFT at the PBE-D2 level of theory to account for the large graphene sheets (see Table S8 and Figure S46). ARES³⁵ is a real-space pseudopotential electronic structure calculation package based on DFT, with highly parallelizable features making the simulation of our system possible. For validation, the real-space DFT (36 C atom CO₂ E_{ads}) calculation is consistent with our exemplary QE calculation at the same level of theory (see Table S1). CO₂ E_{ads} is well-converged for all PG sheet sizes indicating that enthalpy alone does not play a role in coverage. Furthermore, a calculation at a CO₂ concentration of 400 ppm (2211 C atoms/CO₂ molecule) is unnecessary. In addition, we calculated the CO₂ E_{ads} on methylamine and pyridine FG at select coverages. Van der Waals interactions are minimal at 7 Å and negligible >10 Å, corresponding to 60 and 96 C atoms/CO₂ molecule, respectively. CO₂ E_{ads} converges for both methylamine and pyridine FG at a coverage of 60 C atoms/CO₂ molecule (15000 ppm) and lower as the shortest atomic distances between repeating images are ~7 Å. Interestingly, CO₂ is more stable on the 36 C atom sheet (than 60 and 96) of methylamine FG due to O-H interaction of CO₂ and methylamine in repeating images (see Figure S47). To the contrary, CO₂ is less stable on the 36 C atom sheet (than 60 and 96) of pyridine FG due to the H-H interactions of pyridine in repeating images (see Figure S48). Indicating that a higher methylamine coverage (>15000 ppm) and a lower pyridine coverage (<15000 ppm) is preferred for CO₂ adsorption.

Table S8. CO₂ E_{ads} (eV) on PG, NH₂CH₃-FG, and C₅H₅N-FG with respect to coverage

CO ₂ concentration (ppm)	25000	15000	9300	3520	1135	768
# C atoms/CO ₂ molecule	36	60	96	252	780	1152
PG (ARES)	-0.201	-	-	-0.194	-0.196	-0.192
NH ₂ CH ₃ -FG (QE)	-0.357	-0.322	-0.322	-	-	-
C ₅ H ₅ N-FG (QE)	-0.338	-0.352	-0.349	-	-	-

For figures S46-S48, the PG and FG images are in the xz plane view.

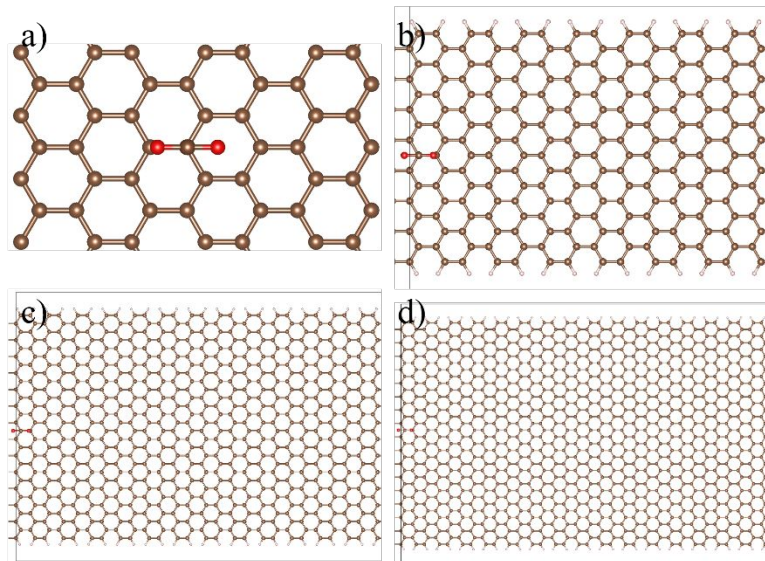


Figure S46. Single point configuration of CO₂ on PG in 36 (a), 252 (b), 780 (c), and 1152 (d) C atom sheets using ARES.

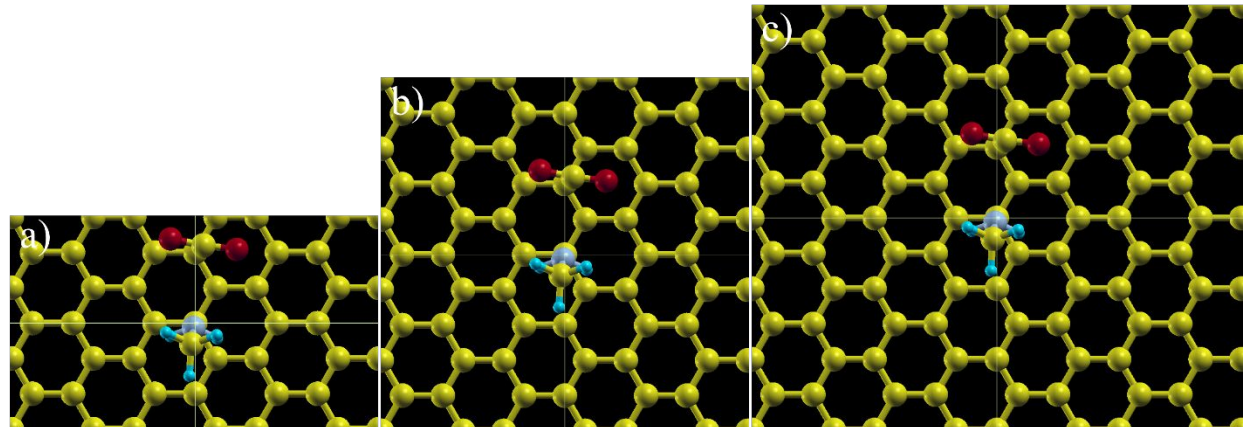


Figure S47. Single point configuration of CO₂ on GNH₂CH₃ in 36 (a), 60 (b), and 96 (c) C atom sheets using QE.

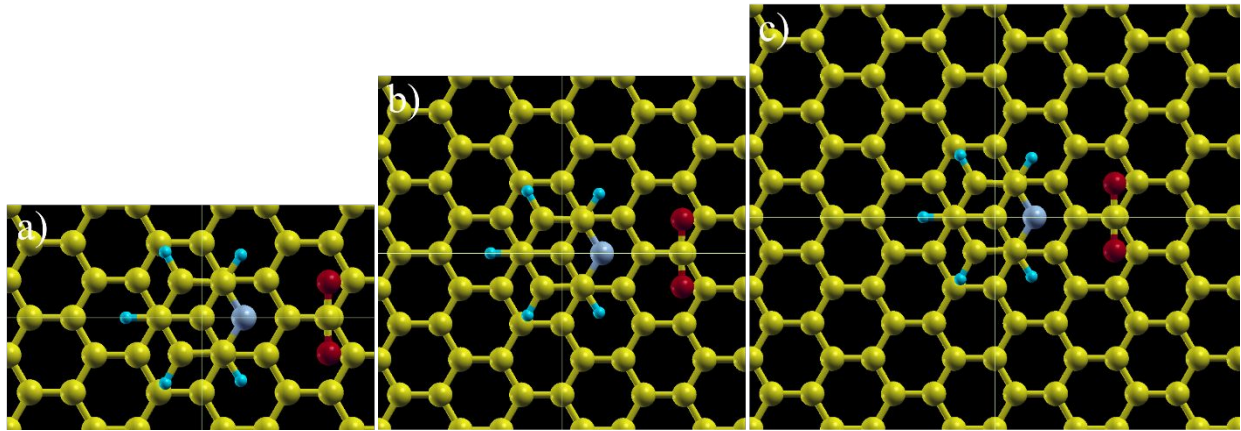


Figure S48. Single point configuration of CO_2 on $\text{GC}_5\text{H}_5\text{N}$ in 36 (a), 60 (b), and 96 (c) C atom sheets using QE.

Van der Waals and Electrostatic Contributions in $\text{CO}_2 E_{\text{ads}}$

To understand our primary criterion of E_{ads} , we investigated the components contributing to E_{ads} in detail. More specifically, $\text{CO}_2 E_{\text{ads}}$ can be decomposed into two major parts: electrostatic and van der Waals (vdW) interactions (see Table S9). The former results largely from the EN difference between the C atom of the CO_2 molecule and the N atom of the functional group, leading to dipole-induced dipole interactions. Thus, to satisfy our primary criteria, CO_2 must have favorable electrostatic interactions with the FMs and π - π dispersion interactions with the graphene surface, and they should add up to our target $\text{CO}_2 E_{\text{ads}}$. Methylamine and pyridine possess favorable electrostatic interactions with CO_2 (-0.15 eV and -0.15 eV), and their vdW interactions with graphene are similar (-0.18 and -0.16 eV, respectively). Interestingly, in both the pyridine and methylamine FG cases, the total, vdW, and ES energy contributions in CO_2 +FM and CO_2 +PG interactions are similar.

Table S9. Interaction energies (eV) of CO_2 with FMs and PG.

Materials	CO_2 +FM			CO_2 +PG		
	Total	vdW	ES	Total	vdW	ES
NH_2CH_3	-0.220	-0.074	-0.146	-0.178	-0.175	-0.003
$\text{C}_5\text{H}_5\text{N}$	-0.216	-0.069	-0.147	-0.171	-0.160	-0.011

Bader Charge Analysis

We investigated the Bader charge difference (BCD) and charge density difference (CDD) for a few N-containing FMs (see Figure 3 and Tables S10-S15). Interestingly, CO₂ is more stable interacting with amine in the inserted site over the top site as the former shows a higher amount of charge transfer compared to the latter. The other N-containing FMs also prefer to interact with CO₂ in the inserted sites. Amine and guanidine formed N-C bonds with CO₂ and show a higher BCD, CDD, and CO₂ E_{ads}, with a lower N-C distance. Although their CO₂ E_{ads} are the same, their BCD and CDD differ because of dissimilar initial Bader charge on N (6.13 e and 7.26 e) despite the final charges being similar (6.82 e and 6.92 e). The initial Bader charge of amine is lower due to the N-C bond formed with C of graphene. Since CO₂ physisorbs on aniline FG, it shows minimal BCD and CDD. Interestingly, pyridine and methylamine also show minimal BCD and CDD. In both cases, C (of CO₂) is favored to interact with N (of methylamine or pyridine) leading to distances of ~2.8 Å, which agrees with the BCD and CDD results.

Table S10. Bader Charge Difference (BCD (e)) for NH₂-T FG

Atom	BC w/ CO ₂	BC	BCD
C	3.91	3.91	0.00
C	4.06	4.04	0.02
C	4.04	4.03	0.00
C	3.92	4.05	-0.13
C	4.06	3.91	0.15
C	4.01	4.03	-0.02
C	4.03	4.01	0.02
C	4.04	4.06	-0.02
C	3.94	3.94	0.00
C	4.01	4.00	0.00
C	4.02	4.02	0.00
C	4.06	4.06	0.00
C	3.91	3.91	0.00
C	3.99	3.99	0.00
C	4.01	4.02	-0.01
C	3.92	4.05	-0.13
C	4.06	3.91	0.15
C	4.00	4.00	0.00
C	4.00	4.00	0.00
C	4.04	4.06	-0.02
C	3.94	3.94	0.00
C	4.00	3.99	0.00
C	4.02	4.02	0.00

C	4.06	4.06	0.00
C	3.56	3.60	-0.04
C	4.06	4.04	0.02
C	4.04	4.03	0.00
C	3.95	3.95	0.01
C	4.03	4.03	0.00
C	4.01	4.03	-0.02
C	4.03	4.01	0.02
C	3.91	3.91	0.01
C	4.04	4.05	-0.01
C	4.01	4.00	0.00
C	4.02	4.02	0.00
C	3.99	3.99	0.00
N	6.16	6.13	0.02
H	0.60	0.59	0.01
H	0.58	0.60	-0.02
C	0.06	0.06	0.00
O	7.96	7.96	0.00
O	7.98	7.98	0.00

Table S11. BCD (e) for C₆H₅NH₂-I FG

Atom	BC w/ CO ₂	BC	BCD
C	3.98	3.98	0.00
C	3.92	3.92	0.00
C	4.05	4.04	0.01
C	4.04	4.04	0.00
C	3.98	3.99	-0.01
C	3.92	3.92	0.00
C	4.05	4.05	0.00
C	4.03	4.03	0.00
C	3.98	3.99	0.00
C	3.92	3.91	0.00
C	4.05	4.05	0.00
C	4.03	4.03	0.00
C	4.02	4.03	0.00
C	3.92	3.93	0.00
C	4.05	4.05	0.00
C	4.03	4.03	0.00
C	4.03	4.03	0.00
C	3.92	3.92	0.00
C	4.05	4.06	-0.01

C	4.01	4.02	0.00
C	4.03	4.03	-0.01
C	3.92	3.92	0.00
C	4.06	4.05	0.00
C	4.02	4.02	0.00
C	4.02	4.02	0.00
C	3.91	3.92	0.00
C	4.03	4.03	0.00
C	4.03	4.03	0.00
C	4.04	4.03	0.01
C	3.92	3.92	0.00
C	4.03	4.04	0.00
C	4.02	4.02	0.01
C	4.03	4.03	0.00
C	3.91	3.91	0.00
C	4.03	4.03	0.00
C	4.01	4.01	0.00
N	6.74	6.76	-0.03
C	3.03	3.02	0.01
C	3.96	4.01	-0.05
C	3.97	4.01	-0.05
C	4.12	4.07	0.05
C	4.12	4.07	0.05
C	4.02	4.03	-0.01
H	0.97	0.97	0.00
H	0.97	0.97	0.00
H	0.96	0.96	-0.01
H	0.96	0.96	-0.01
H	0.98	0.96	0.02
H	0.60	0.59	0.01
H	0.60	0.59	0.01
C	0.07	0.07	0.00
O	7.97	7.96	0.01
O	7.97	7.97	0.01

Table S12. BCD (e) for C₅H₅N-I FG

Atom	BC w/ CO ₂	BC	BCD
C	3.92	3.92	0.00
C	4.03	4.03	0.00
C	4.02	4.02	0.00
C	4.05	4.05	0.00

C	3.91	3.92	0.00
C	4.03	4.03	0.00
C	4.02	4.02	0.00
C	4.05	4.05	0.00
C	3.92	3.92	0.00
C	4.03	4.03	0.00
C	4.02	4.02	0.00
C	4.05	4.05	0.00
C	3.92	3.92	0.00
C	3.99	3.99	0.00
C	4.04	4.04	0.00
C	4.05	4.05	0.00
C	3.91	3.92	0.00
C	3.98	3.98	0.00
C	4.03	4.03	-0.01
C	4.05	4.05	0.00
C	3.92	3.92	0.00
C	3.99	3.98	0.00
C	4.04	4.04	0.00
C	4.05	4.05	0.00
C	3.91	3.91	0.00
C	4.03	4.03	0.00
C	4.02	4.02	0.00
C	4.03	4.03	0.00
C	3.91	3.91	0.01
C	4.03	4.03	0.00
C	4.02	4.02	0.00
C	4.03	4.03	0.00
C	3.91	3.91	0.00
C	4.03	4.03	0.00
C	4.02	4.02	0.00
C	4.03	4.03	0.00
N	7.65	7.67	-0.02
C	4.10	4.04	0.06
C	2.75	2.74	0.01
C	2.75	2.74	0.01
C	4.01	4.04	-0.03
C	4.01	4.04	-0.03
H	0.94	0.94	0.00
H	0.94	0.94	-0.01
H	0.93	0.94	-0.01

H	0.95	0.95	0.00
H	0.95	0.95	0.00
C	0.06	0.07	0.00
O	7.99	7.97	0.02
O	7.98	7.96	0.02

Table S13. BCD (e) for NH₂CH₃-I FG

Atom	BC w/ CO ₂	BC	BCD
C	4.05	4.08	-0.03
C	4.05	4.01	0.03
C	4.04	4.04	0.00
C	3.91	3.91	0.00
C	4.04	4.07	-0.03
C	4.04	4.01	0.02
C	4.03	4.02	0.01
C	3.91	3.92	-0.02
C	4.04	4.07	-0.03
C	4.04	4.01	0.03
C	4.04	4.01	0.02
C	3.91	3.94	-0.03
C	4.06	4.06	0.00
C	4.01	4.01	0.00
C	4.00	4.00	0.00
C	3.92	3.91	0.02
C	4.06	4.07	-0.01
C	4.01	4.01	0.00
C	3.99	4.00	0.00
C	3.94	3.91	0.03
C	4.06	4.07	-0.01
C	4.01	4.00	0.00
C	3.99	4.00	-0.01
C	3.93	3.90	0.03
C	4.04	4.04	0.01
C	4.01	4.00	0.01
C	4.00	4.03	-0.03
C	3.91	3.91	0.00
C	4.04	4.04	0.00
C	4.01	4.01	0.00
C	4.00	4.04	-0.03
C	3.91	3.91	0.00
C	4.04	4.04	0.00

C	4.01	4.01	0.00
C	4.01	4.03	-0.03
C	3.92	3.91	0.01
C	3.64	3.66	-0.02
N	6.05	6.06	-0.01
H	1.03	1.01	0.02
H	0.65	0.65	0.00
H	0.64	0.64	0.00
H	0.98	0.99	-0.01
H	0.98	0.98	0.00
C	0.06	0.07	0.00
O	7.98	7.97	0.02
O	7.99	7.97	0.02

Table S14. BCD (e) for CH₅N₃-I FG

Atom	BC w/ CO ₂	BC	BCD
C	3.91	4.07	-0.16
C	4.04	4.01	0.02
C	4.03	4.02	0.00
C	4.03	3.92	0.11
C	3.91	4.05	-0.14
C	4.04	4.02	0.02
C	4.01	4.02	0.00
C	4.04	3.92	0.12
C	3.91	4.05	-0.15
C	4.04	4.03	0.01
C	4.03	4.04	0.00
C	4.04	3.92	0.12
C	3.90	4.06	-0.16
C	4.02	4.03	-0.02
C	4.00	3.99	0.01
C	4.04	3.91	0.13
C	3.93	4.05	-0.11
C	4.01	4.03	-0.02
C	4.01	3.98	0.03
C	4.06	3.92	0.14
C	3.93	4.05	-0.12
C	4.01	4.03	-0.03
C	4.01	3.99	0.02
C	4.05	3.92	0.13
C	3.92	4.03	-0.12

C	3.99	4.00	-0.01
C	4.02	4.01	0.00
C	4.07	3.91	0.16
C	3.91	4.03	-0.11
C	4.00	4.02	-0.02
C	4.01	4.02	-0.01
C	4.07	3.92	0.15
C	3.91	4.03	-0.12
C	4.00	4.02	-0.03
C	4.02	4.04	-0.02
C	4.07	3.92	0.15
N	7.02	6.86	0.16
N	6.93	6.81	0.11
N	6.92	7.26	-0.33
C	0.06	0.06	0.00
H	0.46	0.57	-0.11
H	0.55	0.60	-0.05
H	0.56	0.59	-0.03
H	0.53	0.60	-0.07
H	0.55	0.64	-0.09
C	0.48	0.06	0.41
O	7.96	7.96	-0.01
O	7.98	7.98	0.00

Table S15. BCD (e) for NH₂-I FG

Atom	BC w/ CO ₂	BC	BCD
C	4.03	3.91	0.12
C	4.03	4.04	-0.01
C	4.02	4.03	-0.01
C	3.91	4.05	-0.14
C	4.03	3.91	0.12
C	4.03	4.03	0.00
C	4.02	4.01	0.01
C	3.90	4.06	-0.16
C	4.04	3.94	0.10
C	4.03	4.00	0.03
C	4.03	4.02	0.01
C	3.90	4.06	-0.16
C	4.03	3.91	0.12
C	4.00	3.99	0.01
C	3.98	4.02	-0.04

C	3.92	4.05	-0.13
C	4.04	3.91	0.13
C	4.01	4.00	0.01
C	4.00	4.00	-0.01
C	3.92	4.06	-0.14
C	4.05	3.94	0.12
C	4.00	3.99	0.00
C	3.99	4.02	-0.03
C	3.89	4.06	-0.16
C	4.02	3.60	0.43
C	4.00	4.04	-0.05
C	3.97	4.03	-0.06
C	3.91	3.95	-0.04
C	4.03	4.03	0.00
C	4.01	4.03	-0.02
C	4.00	4.01	-0.02
C	3.90	3.91	-0.01
C	4.04	4.05	-0.01
C	3.99	4.00	-0.01
C	3.99	4.02	-0.03
C	3.89	3.99	-0.10
N	6.82	6.13	0.69
H	0.59	0.59	0.00
H	0.59	0.60	-0.01
C	0.06	0.07	0.00
O	7.70	7.97	-0.26
O	7.69	7.97	-0.28

References

- (1) Hjorth Larsen, A.; Jørgen Mortensen, J.; Blomqvist, J.; Castelli, I. E.; Christensen, R.; Dułak, M.; Friis, J.; Groves, M. N.; Hammer, B.; Hargus, C.; Hermes, E. D.; Jennings, P. C.; Bjerre Jensen, P.; Kermode, J.; Kitchin, J. R.; Leonhard Kolsbjerg, E.; Kubal, J.; Kaasbjerg, K.; Lysgaard, S.; Bergmann Maronsson, J.; Maxson, T.; Olsen, T.; Pastewka, L.; Peterson, A.; Rostgaard, C.; Schiøtz, J.; Schütt, O.; Strange, M.; Thygesen, K. S.; Vegge, T.; Vilhelmsen, L.; Walter, M.; Zeng, Z.; Jacobsen, K. W. The Atomic Simulation Environment—a Python Library for Working with Atoms. *J. Phys. Condens. Matter* **2017**, *29* (27), 273002. <https://doi.org/10.1088/1361-648X/aa680e>.
- (2) Giannozzi, P.; Baroni, S.; Bonini, N.; Calandra, M.; Car, R.; Cavazzoni, C.; Ceresoli, D.; Chiarotti, G. L.; Cococcioni, M.; Dabo, I.; Dal Corso, A.; de Gironcoli, S.; Fabris, S.; Fratesi, G.; Gebauer, R.; Gerstmann, U.; Gougaoussis, C.; Kokalj, A.; Lazzeri, M.; Martin-Samos, L.; Marzari, N.; Mauri, F.; Mazzarello, R.; Paolini, S.; Pasquarello, A.; Paulatto, L.; Sbraccia, C.; Scandolo, S.; Sclauzero, G.; Seitsonen, A. P.; Smogunov, A.; Umari, P.; Wentzcovitch, C.

- R. M. QUANTUM ESPRESSO: A Modular and Open-Source Software Project for Quantum Simulations of Materials. *J. Phys. Condens. Matter* **2009**, *21* (39), 395502. <https://doi.org/10.1088/0953-8984/21/39/395502>.
- (3) Giannozzi, P.; Andreussi, O.; Brumme, T.; Bunau, O.; Buongiorno Nardelli, M.; Calandra, M.; Car, R.; Cavazzoni, C.; Ceresoli, D.; Cococcioni, M.; Colonna, N.; Carnimeo, I.; Dal Corso, A.; de Gironcoli, S.; Delugas, P.; DiStasio, R. A.; Ferretti, A.; Floris, A.; Fratesi, G.; Fugallo, G.; Gebauer, R.; Gerstmann, U.; Giustino, F.; Gorni, T.; Jia, J.; Kawamura, M.; Ko, H.-Y.; Kokalj, A.; Küçükbenli, E.; Lazzeri, M.; Marsili, M.; Marzari, N.; Mauri, F.; Nguyen, N. L.; Nguyen, H.-V.; Otero-de-la-Roza, A.; Paulatto, L.; Poncé, S.; Rocca, D.; Sabatini, R.; Santra, B.; Schlipf, M.; Seitsonen, A. P.; Smogunov, A.; Timrov, I.; Thonhauser, T.; Umari, P.; Vast, N.; Wu, X.; Baroni, S. Advanced Capabilities for Materials Modelling with Quantum ESPRESSO. *J. Phys. Condens. Matter* **2017**, *29* (46), 465901. <https://doi.org/10.1088/1361-648X/aa8f79>.
- (4) Giannozzi, P.; Baseggio, O.; Bonfà, P.; Brunato, D.; Car, R.; Carnimeo, I.; Cavazzoni, C.; de Gironcoli, S.; Delugas, P.; Ferrari Ruffino, F.; Ferretti, A.; Marzari, N.; Timrov, I.; Urru, A.; Baroni, S. Q UANTUM ESPRESSO toward the Exascale. *J. Chem. Phys.* **2020**, *152* (15), 154105. <https://doi.org/10.1063/5.0005082>.
- (5) Grimme, S. Semiempirical GGA-Type Density Functional Constructed with a Long-Range Dispersion Correction. *J. Comput. Chem.* **2006**, *27* (15), 1787–1799. <https://doi.org/10.1002/jcc.20495>.
- (6) Barone, V.; Casarin, M.; Forrer, D.; Pavone, M.; Sambi, M.; Vittadini, A. Role and Effective Treatment of Dispersive Forces in Materials: Polyethylene and Graphite Crystals as Test Cases. *J. Comput. Chem.* **2009**, *30* (6), 934–939. <https://doi.org/10.1002/jcc.21112>.
- (7) Blöchl, P. E. Projector Augmented-Wave Method. *Phys. Rev. B* **1994**, *50* (24), 17953–17979. <https://doi.org/10.1103/PhysRevB.50.17953>.
- (8) van Setten, M. J.; Giantomassi, M.; Bousquet, E.; Verstraete, M. J.; Hamann, D. R.; Gonze, X.; Rignanese, G.-M. The PseudoDojo: Training and Grading a 85 Element Optimized Norm-Conserving Pseudopotential Table. *Comput. Phys. Commun.* **2018**, *226*, 39–54. <https://doi.org/10.1016/j.cpc.2018.01.012>.
- (9) Henkelman, G.; Arnaldsson, A.; Jónsson, H. A Fast and Robust Algorithm for Bader Decomposition of Charge Density. *Comput. Mater. Sci.* **2006**, *36* (3), 354–360. <https://doi.org/10.1016/j.commatsci.2005.04.010>.
- (10) Sanville, E.; Kenny, S. D.; Smith, R.; Henkelman, G. Improved Grid-Based Algorithm for Bader Charge Allocation. *J. Comput. Chem.* **2007**, *28* (5), 899–908. <https://doi.org/10.1002/jcc.20575>.
- (11) Tang, W.; Sanville, E.; Henkelman, G. A Grid-Based Bader Analysis Algorithm without Lattice Bias. *J. Phys. Condens. Matter* **2009**, *21* (8), 084204. <https://doi.org/10.1088/0953-8984/21/8/084204>.
- (12) Yu, M.; Trinkle, D. R. Accurate and Efficient Algorithm for Bader Charge Integration. *J. Chem. Phys.* **2011**, *134* (6), 064111. <https://doi.org/10.1063/1.3553716>.
- (13) Momma, K.; Izumi, F. VESTA 3 for Three-Dimensional Visualization of Crystal, Volumetric and Morphology Data. *J. Appl. Crystallogr.* **2011**, *44*, 1272–1276. <https://doi.org/10.1107/S0021889811038970>.
- (14) Patel, H. A.; Byun, J.; Yavuz, C. T. Carbon Dioxide Capture Adsorbents: Chemistry and Methods. *ChemSusChem* **2017**, *10* (7), 1303–1317. <https://doi.org/10.1002/cssc.201601545>.

- (15) Koh, H. S.; Rana, M. K.; Hwang, J.; Siegel, D. J. Thermodynamic Screening of Metal-Substituted MOFs for Carbon Capture. *Phys. Chem. Chem. Phys.* **2013**, *15* (13), 4573. <https://doi.org/10.1039/c3cp50622c>.
- (16) American Physical Society. *Direct Air Capture of CO₂ with Chemicals*; A Technology Assessment for the APS Panel on Public Affairs; 2011. <https://www.aps.org/policy/reports/assessments/upload/dac2011.pdf>.
- (17) Wang, C.; Fang, Y.; Duan, H.; Liang, G.; Li, W.; Chen, D.; Long, M. DFT Study of CO₂ Adsorption Properties on Pristine, Vacancy and Doped Graphenes. *Solid State Commun.* **2021**, *337*, 114436. <https://doi.org/10.1016/j.ssc.2021.114436>.
- (18) Wood, B. C.; Bhide, S. Y.; Dutta, D.; Kandagal, V. S.; Pathak, A. D.; Punnathanam, S. N.; Ayappa, K. G.; Narasimhan, S. Methane and Carbon Dioxide Adsorption on Edge-Functionalized Graphene: A Comparative DFT Study. *J. Chem. Phys.* **2012**, *137* (5), 054702. <https://doi.org/10.1063/1.4736568>.
- (19) Zheng, Z.; Wang, H. Different Elements Doped Graphene Sensor for CO₂ Greenhouse Gases Detection: The DFT Study. *Chem. Phys. Lett.* **2019**, *721*, 33–37. <https://doi.org/10.1016/j.cplett.2019.02.024>.
- (20) Shokuhi Rad, A.; Pouralijan Foukolaei, V. Density Functional Study of Al-Doped Graphene Nanostructure towards Adsorption of CO, CO₂ and H₂O. *Synth. Met.* **2015**, *210*, 171–178. <https://doi.org/10.1016/j.synthmet.2015.09.026>.
- (21) Cortés-Arriagada, D.; Villegas-Escobar, N.; Ortega, D. E. Fe-Doped Graphene Nanosheet as an Adsorption Platform of Harmful Gas Molecules (CO, CO₂, SO₂ and H₂S), and the Co-Adsorption in O₂ Environments. *Appl. Surf. Sci.* **2018**, *427*, 227–236. <https://doi.org/10.1016/j.apsusc.2017.08.216>.
- (22) Mason, J. A.; Sumida, K.; Herm, Z. R.; Krishna, R.; Long, Jeffrey. R. Evaluating Metal-Organic Frameworks for Post-Combustion Carbon Dioxide Capture via Temperature Swing Adsorption. *Energy Environ. Sci.* **2011**, *4* (8), 3030. <https://doi.org/10.1039/c1ee01720a>.
- (23) Fu, Y.; Yao, Y.; Forse, A. C.; Li, J.; Mochizuki, K.; Long, J. R.; Reimer, J. A.; De Paëpe, G.; Kong, X. Solvent-Derived Defects Suppress Adsorption in MOF-74. *Nat. Commun.* **2023**, *14* (1), 2386. <https://doi.org/10.1038/s41467-023-38155-8>.
- (24) Caskey, S. R.; Wong-Foy, A. G.; Matzger, A. J. Dramatic Tuning of Carbon Dioxide Uptake via Metal Substitution in a Coordination Polymer with Cylindrical Pores. *J. Am. Chem. Soc.* **2008**, *130* (33), 10870–10871. <https://doi.org/10.1021/ja8036096>.
- (25) Britt, D.; Furukawa, H.; Wang, B.; Glover, T. G.; Yaghi, O. M. Highly Efficient Separation of Carbon Dioxide by a Metal-Organic Framework Replete with Open Metal Sites. *Proc. Natl. Acad. Sci.* **2009**, *106* (49), 20637–20640. <https://doi.org/10.1073/pnas.0909718106>.
- (26) Deng, H.; Grunder, S.; Cordova, K. E.; Valente, C.; Furukawa, H.; Hmadeh, M.; Gándara, F.; Whalley, A. C.; Liu, Z.; Asahina, S.; Kazumori, H.; O’Keeffe, M.; Terasaki, O.; Stoddart, J. F.; Yaghi, O. M. Large-Pore Apertures in a Series of Metal-Organic Frameworks. *Science* **2012**, *336* (6084), 1018–1023. <https://doi.org/10.1126/science.1220131>.
- (27) McDonald, T. M.; Mason, J. A.; Kong, X.; Bloch, E. D.; Gygi, D.; Dani, A.; Crocellà, V.; Giordanino, F.; Odoh, S. O.; Drisdell, W. S.; Vlaisavljevich, B.; Dzubak, A. L.; Poloni, R.; Schnell, S. K.; Planas, N.; Lee, K.; Pascal, T.; Wan, L. F.; Prendergast, D.; Neaton, J. B.; Smit, B.; Kortright, J. B.; Gagliardi, L.; Bordiga, S.; Reimer, J. A.; Long, J. R. Cooperative Insertion of CO₂ in Diamine-Appended Metal-Organic Frameworks. *Nature* **2015**, *519* (7543), 303–308. <https://doi.org/10.1038/nature14327>.

- (28) Vlaisavljevich, B.; Huck, J.; Hulvey, Z.; Lee, K.; Mason, J. A.; Neaton, J. B.; Long, J. R.; Brown, C. M.; Alfè, D.; Michaelides, A.; Smit, B. Performance of van Der Waals Corrected Functionals for Guest Adsorption in the M_2 (Dobdc) Metal–Organic Frameworks. *J. Phys. Chem. A* **2017**, *121* (21), 4139–4151. <https://doi.org/10.1021/acs.jpca.7b00076>.
- (29) Lee, J.-H.; Siegelman, R. L.; Maserati, L.; Rangel, T.; Helms, B. A.; Long, J. R.; Neaton, J. B. Enhancement of CO_2 Binding and Mechanical Properties upon Diamine Functionalization of M_2 (Dobpdc) Metal–Organic Frameworks. *Chem. Sci.* **2018**, *9* (23), 5197–5206. <https://doi.org/10.1039/C7SC05217K>.
- (30) Takeuchi, K.; Yamamoto, S.; Hamamoto, Y.; Shiozawa, Y.; Tashima, K.; Fukidome, H.; Koitaya, T.; Mukai, K.; Yoshimoto, S.; Suemitsu, M.; Morikawa, Y.; Yoshinobu, J.; Matsuda, I. Adsorption of CO_2 on Graphene: A Combined TPD, XPS, and vdW-DF Study. *J. Phys. Chem. C* **2017**, *121* (5), 2807–2814. <https://doi.org/10.1021/acs.jpcc.6b11373>.
- (31) Lee, H. M.; Youn, I. S.; Saleh, M.; Lee, J. W.; Kim, K. S. Interactions of CO_2 with Various Functional Molecules. *Phys. Chem. Chem. Phys.* **2015**, *17* (16), 10925–10933. <https://doi.org/10.1039/C5CP00673B>.
- (32) Bénard, P.; Chahine, R. Carbon Nanostructures for Hydrogen Storage. In *Solid-State Hydrogen Storage*; Elsevier, 2008; pp 261–287. <https://doi.org/10.1533/9781845694944.3.261>.
- (33) Swenson, H.; Stadie, N. P. Langmuir's Theory of Adsorption: A Centennial Review. *Langmuir* **2019**, *35* (16), 5409–5426. <https://doi.org/10.1021/acs.langmuir.9b00154>.
- (34) Ganesan, A.; Shaijumon, M. M. Activated Graphene-Derived Porous Carbon with Exceptional Gas Adsorption Properties. *Microporous Mesoporous Mater.* **2016**, *220*, 21–27. <https://doi.org/10.1016/j.micromeso.2015.08.021>.
- (35) Xu, Q.; Wang, S.; Xue, L.; Shao, X.; Gao, P.; Lv, J.; Wang, Y.; Ma, Y. *Ab Initio* Electronic Structure Calculations Using a Real-Space Chebyshev-Filtered Subspace Iteration Method. *J. Phys. Condens. Matter* **2019**, *31* (45), 455901. <https://doi.org/10.1088/1361-648X/ab2a63>.